Geologia Croatica
Journal of the Croatian Geological Survey and the Croatian Geological Society

2020 | 73/1 | 29–48 | 12 Figs. | 14 Tabs. | www.geologia-croatica.hr

Comprehensive characterisation of bentonites from Croatia and neighbouring countries

Zvonka Gverić[1], Darko Hanžel[2], Štefica Kampić[1], Andrej Pleša[3] and Darko Tibljaš*[,1]

[1] University of Zagreb, Faculty of Science, Department of Geology, Division of Mineralogy and Petrology, Horvatovac 95, HR-10 000, Zagreb, Croatia; (*corresponding author: dtibljas@geol.pmf.hr)
[2] Jožef Stefan Institute, Jamova cesta 39, SI-1000 Ljubljana, Slovenia
[3] INA d.d., Exploration and production, Avenija Većeslava Holjevca 10, HR-10 000, Zagreb, Croatia

doi: 10.4154/gc.2020.02

Crossref Similarity Check

Article history:

Manuscript received September 25, 2019
Revised manuscript accepted January 17, 2020
Available online February 29, 2020

Abstract

Bentonites are an important industrial resource and are also interesting from the mineralogical point of view. The main component of bentonites is a mineral from the smectite group in which chemical and structural variations, influencing bentonite properties, provide a great deal of interesting research topics. The aim of this study was to better describe bentonites from 11 known deposits from Croatia and neighbouring countries: Bednja, Bunarić, Draga, Divoselo, Sjeničak, Paripovac, Lončarski vis and Poljanska Luka (Croatia), Zaloška Gorica (Slovenia), Šipovo (Bosnia and Herzegovina) and Vranjska Banja (Serbia). Thirteen samples were analysed using several available techniques in order to obtain the data necessary for currently accepted bentonite classification. The mineralogical composition was analysed using XRD and FTIR, and crystallo-chemical properties were investigated by thermal analysis, CEC determination with ammonium index cations, chemical analyses (ICP-AES and ICP-MS) and Mössbauer spectroscopy. The results showed that the main mineral constituent of most local bentonite deposits is a Fe-poor smectite, with a predominantly medium layer charge mostly as a result of octahedral substitutions, with calcium or sodium cations occupying the interlayer. Nevertheless, the variations between samples are prominent enough to provide a good overview of the range of crystallo-chemical properties which exist in different smectites resulting in varying bentonite properties.

Keywords: bentonite deposits, smectite crystallo-chemical properties

1. INTRODUCTION

There are several bentonite deposits and occurrences in Croatia and neighbouring countries formed by alteration of volcanic ash, in different geological settings with ages ranging from the Late Jurassic to the Middle Miocene.

Some of these deposits were exploited in the past, and with technological advancements and new applications emerging, some of them could be economically viable again. Bentonite is used for numerous purposes, most commonly in drilling fluids, metal castings, civil-engineering, as pet-waste adsorbents, desiccants, environmental sealants etc. Other uses of bentonite, including the pharmaceutical and cosmetic industries, nanotechnology and various other uses, such as barrier materials for storing nuclear waste or removing contaminants from wastewater, are gaining momentum. Such diversity and abundance of possible applications calls for a thorough understanding of bentonite, including its different types and properties.

Properties of different bentonites vary widely because of the variations in their mineralogical composition. The smectite species is the most important factor determining bentonite properties, such as adsorption capacity or swelling behaviour. As the main constituent and the one giving bentonite its specific characteristics, smectite is the obvious object of interest in most of the research done on bentonites.

Different types of smectites were distinguished by GRIM & KULBICKI (1961), SCHULTZ (1969), BRIGATTI & POPPI (1981), and BRIGATTI (1983). They proposed trivial names, derived from the provenance of the most typical samples, such as Wyoming, Tatatilla, Chambers, and Otay (Cheto), which differ in layer charge (particularly in its value and whether it originates from substitutions in the tetrahedral or octahedral sheets), high-temperature transformations, and Fe content. Unfortunately, these trivial names do not reflect some of the important chemical and structural parameters. Furthermore, several montmorillonites could not be assigned to the proposed types according to this classification system. Therefore EMMERICH et al. (2009) proposed a new comprehensive classification, which allowed modifications and extension of the old one. It is based on the chemical composition (tetrahedral/octahedral charge distribution), the layer charge and exchangeable cations, the di- and trioctahedral character, Fe content and the structure of the octahedral sheet (cis-, trans-vacancy). The new classification (which is also used here) is based on standardised laboratory techniques used in characterisation of smectites.

The most extensive research on bentonites in Croatia was done by BRAUN (1991) and it has served as a foundation for many later works. Some of the other research was undertaken for industrial purposes, which goes along with the fact that 9 samples (from 7 locations) used in this study were taken from active or once active bentonite mines where bentonite was used in drilling fluids and castings. The data gathered from this industrial-based research has been compiled by MARKOVIĆ (2002). Additionally, bentonite deposits in the north-eastern part of Croatia have been studied by TIBLJAŠ (1996), and those in south Croatia by ŠEGVIĆ et al. (2006) and BIŠEVAC et al. (2007).

Samples of bentonite contain different smectite, resulting in their varying properties. Considering the large array of possibilities for bentonite use, it is important to be able to choose the

sample with desirable properties appropriate for the specific application. Consequently, an accurate identification and classification of the different smectites is important and the aim of this study was to reinvestigate Croatian bentonites by several available techniques and methods, and classify them in accordance with the criteria from contemporary literature. For comparison, a few samples of bentonites of similar ages from neighbouring countries were also studied.

2. GEOLOGICAL SETTING

The investigated bentonites differ in age and depositional environments (Fig. 1, Table 1) whereby the oldest, Bunarić (from the Maovice-Štikovo area), located in the External Dinarides, was deposited in Late Jurassic (Malmian-Kimmeridgian) Lemeš beds. The sedimentary succession, consisting of light-coloured platy limestone and/or dolomitic limestone and dolomite with chert intercalations, formed on the Adriatic Carbonate Platform in an intraplatform trough, connected to the open Tethyan realm (VLAHOVIĆ et al., 2005). Two bentonite layers exist within the succession, separated by 4 to 6 m of limestone and chert. The lower layer is approx. 3.5 m thick while the thickness of the upper layer varies between 1.5 and 5.5 m (BRAUN, 1991).

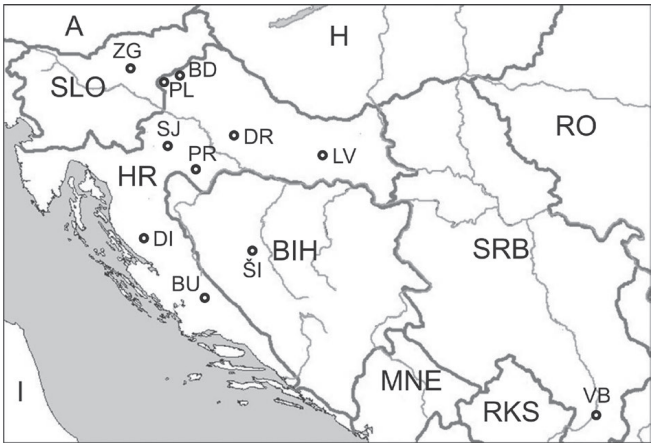

Figure 1. Sampling locations (abbreviations defined in Table 1), A = Austria; BIH = Bosnia and Herzegovina; H = Hungary; HR = Croatia, I = Italy; MNE = Montenegro; RKS = Kosovo; SLO = Slovenia; SRB = Serbia.

Table 1. List of samples.

Sample	Sampling location	Age
BU	Bunarić, Central Dalmatia, S Croatia	Late Jurassic (Kimmeridgian) (BRAUN, 1991)
ZG*	Zaloška Gorica, E Slovenia	Oligocene (RIHTERŠIČ, 1958)
BD	Bednja, Hrvatsko zagorje, NW Croatia	Early Miocene (Eggenburgian-Ottnangian) (BRAUN, 1991)
DR	Draga, Moslavina, Central Croatia	Early Miocene (Ottnangian) (BRAUN, 1991)
ŠI1	Sokolac, Šipovo, Central Bosnia and Herzegovina	Early Miocene (KRSTIĆ et al., 2001)
ŠI2	Greda, Šipovo, Central Bosnia and Herzegovina	Early Miocene (KRSTIĆ et al., 2001)
SJ	Sjeničak, Central Croatia	Middle Miocene (Badenian) (MANDIC et al., 2012)
PR	Paripovac, Central Croatia	Middle Miocene (Badenian) (MANDIC et al., 2012)
DI1	Divoselo, Lika, SW Croatia	unknown
DI2	Divoselo, Lika, SW Croatia	unknown
LV	Lončarski vis, Slavonija, E Croatia	Early Miocene (Karpatian) (MARKOVIĆ et al., 2018)
VB*	Vranjska Banja, SE Serbia	Early to Middle Miocene (KRSTIĆ et al., 2001)
PL	Poljanska Luka, Hrvatsko zagorje, NW Croatia	Middle Miocene (Badenian) (BRAUN, 1991)

*samples from the collection of the Division of Mineralogy and Petrology, Faculty of Science.

Bentonites from Zaloška Gorica and Bednja were deposited during the Oligocene and the Early Miocene (Eggenburgian), respectively, in the Slovenia-Zagorje Basin (SZB). The SZB is also known as the Trans-Tethyan Trench Corridor which acted as a marine connection between the Paratethys and the Mediterranean (RÖGL, 1998). This region formed prior to the Southern Pannonian Basin (SPB) installation at the south-eastern margin of the Paratethys Basin (MANDIC et al., 2012).

The Zaloška Gorica deposit is located in the northern part of the Celje Basin within a bentonite belt extending for 15 km. The bentonite occurs in three exploitable layers in the upper part of an andesitic tuff horizon which is up to 100 m thick and is intercalated with the Oligocene clays overlying Triassic rocks. These clays are conformably overlain by the Badenian lithothamnium sandstones and conglomerates and quartz sands as the youngest Miocene sediments (RIHTERŠIČ, 1958; DRŽAJ & LUKACS, 1968).

In the Bednja area (known for its bentonite deposits), the Šaša clay pit is the largest. The irregular plate-shaped bentonite body which occurs there is 10 to 35 m thick and 165 m wide, tectonically embedded within coarse-grained marine arenites. The body is composed of a random mixture of different varieties of altered pyroclastic rocks: volcanic agglomerates, lapilli tuff, banded and pelitic tuff (BRAUN, 1991). Based on the fossil content and superposition, the sediments were deposited during the Late Eggenburgian-Early Ottnangian and belong to the Vrbno Member of the Macelj Formation (AVANIĆ, 2012).

Another group of deposits was formed in the SPB, prior to Paratethys flooding, in lakes closely related to the Dinaride Lake System (DLS) (MANDIC et al., 2012 and references therein). In the area around Gornja Jelenska, bentonite clays, formed by the alteration of andesitic vitroclastic tuff, were discovered in several deposits. A sample from the Draga deposit was used in this study. According to BRAUN (1991), three bentonite layers (0.15-0.9 m, 0.2-1.2 m and 0-2.0 m thick) occur in continental, most probably lacustrine Ottnangian, strongly tectonized sediments, represented by gravel, sand, silt, sandy and tuffitic marl, tuffite and sandy clay which alternate both vertically and laterally. All three bentonite layers have a sharp contact with the underlying layer, while they gradually transit to tuffite in the overlying layer. Based on palynological analyses, KRIZMANIĆ (1995) concluded that the bentonite was deposited during the Late Karpatian to the Early Badenian in a swamp with gently inclined shores, but with deeper water areas.

In the area around Šipovo (Bosnia and Herzegovina), several bentonite deposits (VUJNOVIĆ, 1981) formed in the intra-montaine basin of the DLS (KRSTIĆ et al., 2001, 2003). In the Grabež and Sarići deposits, three bentonite layers are underlain by Lower Miocene sandy clay. The bentonite layers (approximately 2.5, 2 and 5.5 m thick) are separated by 1 - 5 m of clastic rocks. To the south, in the Babići and Greda deposits, two bentonite layers were described by MILADINOVIĆ (1976) and VUJNOVIĆ (1981). There are some controversies concerning their age. According to literature, they were deposited in the Middle Miocene (MILADINOVIĆ, 1976), Middle to Late Miocene (VUJNOVIĆ, 1981) or even the Late Miocene (TRUBELJA & BARIĆ, 1979), but the newest palaeontological data (KRSTIĆ et al., 2001 and references therein)

show that the lacustrine sediments were deposited in the middle Early Miocene, i.e. between 19 and 17 Ma ago.

Other lacustrine deposits are observable at Sjeničak and Paripovac (30 km apart), in the Karlovac and Glina sub-depressions where a 0.5 m thick altered volcanic ash occurs in the upper part of the sediments deposited in the Early Badenian (≈16.0 Ma, based on $^{40}Ar/^{39}Ar$ dating). In Sjeničak, the bentonite is represented by a biotite-bearing montmorillonite clay layer, underlain by more than 6 m of interbedded sands, pelites and limestone, and is positioned 2 m below the transgression horizon, marked by a marine organogenic limestone of Badenian age. In Paripovac, the ash is grey, medium-size sand, with white calcite veins and biotite flakes. It is intercalated in a sedimentary sequence consisting of 2 m of clays and silts below the ash and about 1 m of clays and lacustrine limestone above the ash deposit (MANDIC et al., 2012).

Bentonite from Divoselo most probably also belongs to this group of deposits, based on the similarity of the tuff mineral associations and mineral morphology with those from Neogene basins in Dalmatia, although its age and depositional environment is unknown. Clays were discovered under a thin Quaternary cover on the palaeorelief formed on Malmian carbonates. In the boreholes, usually one to three bentonite layers occur in the first 10 m (0.3-0.5, 1.6-2.0 and approx. 2 m thick). These are separated by tuff layers, though sometimes due to erosion the first one or two layers are missing. In one of the deeper boreholes, a 13.2 m thick clay layer was observed, and in another, bentonite clay was observed at a depth of 24.3 m (MARKOVIĆ, 2002).

In the SPB, bentonites were also formed in marine environments. In Lončarski vis, (an area close to Gradac village), there are several quartz-trachyandesite quarries. Apart from the main volcanic body, smaller flows and tuff layers are interstratified within Karpatian marine sediments (breccia-conglomerates, gravels, sands and marls) (PAMIĆ, 1997 and references therein). Some tuff layers are altered to bentonite. Radiometric dating using $^{40}Ar/^{39}Ar$ dated tuffs at 16.96 ± 0.03 Ma, corresponding to Karpatian age (MARKOVIĆ et al., 2018).

The Poljanska Luka bentonite deposit, also formed in the SPB after the Paratethys flooding, and contains four beds of bentonite clay as a result of the alteration of vitroclastic tuff. Two lower layers, between 0.6 and 1 m thick, extend over 1800 m and were previously exploited. They are bound on the upper and lower surfaces by 0.5 m thick layers of altered tuffite. Bentonites are interstratified in Badenian marls, calcilutites and biomicrites, which were deposited in a lagoon environment (BRAUN, 1991; MARKOVIĆ, 2002).

The bentonite sample from Vranjska Banja (Serbia) was taken from the collection of the Division of Mineralogy and Petrology at the Faculty of Science, University of Zagreb, so its exact geographic and stratigraphic positions are unknown. It originates from the area in which pyroclastic material is widespread and is better known for zeolite than bentonite deposits (SIMIĆ, 2001; SIMIĆ et al. 2014). According to KRSTIĆ et al. (2001) a large outcrop from Vranje to Vranjska Banja with prevailing tuff layers and subordinate tuffaceous sandstones and breccias, and an andesite lava flow, formed in a fresh water lacustrine environment (Serbian Lake) during the transition from the Lower into the Middle Miocene. According to the older sources (VUKANOVIĆ et al., 1977) this outcrop belongs to the Upper Eocene sedimentary succession within the Pčinja Palaeogene Basin comprising up to 750 m of pyroclastic rocks. The pyroclastics were deposited on land and in shallow fresh water (lacustrine, braided river) environments which prograded into a marine one.

3. MATERIALS AND METHODS

The bentonite samples used in this study, named after the locations where they were collected from are: Bednja, Poljanska Luka, Draga, Lončarski vis, Paripovac, Sjeničak, Bunarić, two samples from Divoselo (Croatia); two samples from Šipovo (Bosnia and Herzegovina); Vranjska Banja (Serbia) and Zaloška Gorica (Slovenia) (Fig. 1, Table 1).

Preparation of the samples included either grinding in an agate mortar to prepare whole rock (WR) samples or separation of the clay-size (< 2 μm) fraction by centrifugation. Approximately 50 g of sample was dispersed in approximately 600 ml of distilled water, then the resulting slurry was centrifuged using a Tehtnica Centric 322A machine at configuration (time calculated using Centrifuge software (KRUMM, 1994). The suspended clay-size particles were taken from the top of the suspension. WR samples were used to determine the mineral composition (XRD), cation exchange capacity (CEC) and chemical composition, while the clay-size fraction was used for clay mineral determination (XRD), FTIR analysis, chemical analysis, determination of the structural iron characteristics and thermal properties.

3.1. X-ray diffraction (XRD)

XRD analyses were performed on both WR and clay-size fraction samples using a Philips PW3040/60 X'Pert PRO diffractometer equipped with Cu tube (40 kV and 40 mA), graphite monochromator and proportional counter. The following slits were used: mask 10 mm, 1/2° divergence slit, 1° and 2° antiscatter slits on tube and detector side respectively, and a 0.2 mm receiving slit. The samples were scanned in continuous mode at a speed of 0.02 °2θ/s. Diffraction patterns were processed using an X'Pert HighScore computer program (PANanalytical, 2004) and compared with the Powder Diffraction File database and with the data from literature (BROWN, 1961; BRINDLEY & BROWN, 1980; MOORE & REYNOLDS, 1997). The clay-size fraction (< 2 μm) was analysed as a randomly oriented powder and was also used to make oriented mounts on glass slides (after MOORE & REYNOLDS, 1997). Oriented samples were analysed as air-dried, after leaving the glass slides overnight in ethylene glycol vapour, and after heating for 1 h at 400 °C and 550 °C. Clay minerals were identified by observing changes on diffractograms after different treatments using the flowchart from STARKEY et al. (1984).

To differentiate between smectites and vermiculites, montmorillonite and beidellite, and to estimate the layer charge, clay-size fractions were treated with magnesium, lithium and potassium chloride solutions (concentrations: 3M for lithium chloride and 1M for magnesium and potassium chloride solutions). Approximately 200 mg of the sample (<2 μm fraction) was mixed with 30 ml of solution (done separately for each chloride solution) in cuvettes and left overnight on a shaker at 250 rpm. The suspension was then centrifuged at 3500 rpm for 15 minutes, the supernatant then decanted and the sample washed three times with ethanol solution (80%). Materials saturated with a cation of interest were dispersed in a few drops of distilled water and analysed as oriented glass slide mounts using XRD. Magnesium saturated samples were solvated with glycerol following the procedure proposed by ŚRODOŃ (1980), i.e. left overnight covered with glycerol-soaked filter paper. Lithium saturated samples were heated to 200 °C and treated with glycerol (again covered overnight with glycerol-soaked filter paper) following GREENE-KELLY (1955). The approximate layer charge was inferred using part of the method described by CHRISTIDIS & EBERL (2003). The swelling behaviour of potassium saturated samples, which were fully expandable in the original form was observed, adopting the prin-

ciple that low-charge smectites would swell to >16.6 Å after 12+ hours in a desiccator with ethylene-glycol vapours, while the high-charged ones would show a basal peak between 13.5 and 15.5 Å.

A randomly oriented clay-size powder was additionally analysed in step-scan mode (step 0.02 °2Θ, time 5 s) in the range from 58.5 to 64.5 °2Θ to measure 060 peak positions and determine the *b* cell dimension (by multiplying d_{060} by 6). Quartz was used as an external standard.

3.2. Fourier Transform Infrared (FTIR) spectroscopy

Approximately 2 mg of the clay size fraction was mixed with approximately 200 mg of KBr powder, homogenized and pressed into pellets with a diameter of 13 mm. The spectra were recorded immediately after pressing, after which the pellets were heated at 150 °C overnight and cooled down in a desiccator before repeated recording.

The spectra were obtained using a Bruker TENSOR 27 FTIR spectrometer equipped with a KBr beam splitter. Thirty-two scans in the MIR (4000 – 400 cm^{-1}) region were recorded for each sample with a resolution of 2 cm^{-1}. The spectra were interpreted using data from the literature (MADEJOVÁ & KOMADEL, 2001; RUSSELL & FRASER, 1994).

3.3. CEC determination

NH_4^+ ions were used as index cations to determine the cation exchange capacity following the procedure proposed by MINATO (1997) for zeolites. Homogenized portions of the WR sample (1 g) were dried and suspended in 30 ml 1M ammonium acetate solution. After mixing, the suspension was centrifuged at 3500 rpm for 17 minutes and the precipitate was washed three times with ethanol. NH_4^+ cations were then exchanged with potassium cations using 30 ml 1M potassium chloride solution, centrifuged at 3500 rpm for 8 minutes and the supernatant was preserved. This was repeated three times for each sample. The released ammonium cations were measured using a Hach ammonium probe.

3.4. Thermal analyses

Six samples (BD, BU, DI 1, DR, PL and ŠI 1) of about 20 mg were analysed using a Shimadzu TG/DTA instrument. The heating rate was 20 K/min in the 30 – 1000 °C range. The analysis was performed in an air current (flow rate: 100 ml/min), samples were placed in platinum crucibles and an empty crucible was used as a reference material. The instrument was calibrated using indium, tin and aluminium for temperature and DTA correction.

The remaining 7 samples were analysed using a Mettler Toledo TG/SDTA 851e. The heating rate was 10 K/min in the 30 – 1000 °C range. Samples (around 35 mg of each) were analysed in aluminium oxide crucibles in an oxygen atmosphere (flow rate: 150 ml/min) while nitrogen was used as a protective gas (50 ml/min). An empty crucible was used as a reference material.

Dehydration and dehydroxylation temperatures were read by observing the peak positions on DTA/DTG curves, no peak decomposition was made.

3.5. Chemical analysis

Major and trace elements both in the WR and clay-size fraction of the samples were analysed using ICP-AES (Spectro Ciros Vision instrument) and ICP-MS (Elan 9000 instrument) in the Bureau Veritas Mineral Laboratories (Vancouver, Canada). The sample weight used was 0.2 g for each analysis. For major and some trace element analysis samples were fused with lithium metaborate and tetraborate and dissolved in diluted nitric acid. Other trace elements (Au, Ag, As, Bi, Cd, Cu, Hg, Mo, Ni, Pb, Sb, Se, Tl and Zn) were analysed using ICP-MS after the samples were dissolved in aqua regia. Carbon and sulfur were analysed on Leco Induction furnace CS230 and LOI was determined after burning the sample at 1000 °C.

The chemical composition of the <2 μm fraction was used to calculate the chemical formulae of the samples. Considering the impurities found in this fraction (both by XRD and FTIR methods), corrections for the crystalline impurities were made. Their quantities were assumed based on XRD peak intensities and for some samples a trial-and-error type deduction, necessary to obtain reasonable formulae (e.g. Si<4, sum of octahedral cations = 2, charge balance of the layer and interlayer cations) was undertaken. Mostly, the impurities were present only in relatively small amounts.

The corrected chemical composition was then used to calculate the structural formula based on half a unit cell with $O_{10}OH_2$ and 22 negative charges and calculated after STEVENS (1946). Cations were appointed to different positions as follows:

– all Si atoms were assigned to the tetrahedral sheet
– the rest of the spaces in the tetrahedral sheet were given to Al or Al and Fe^{3+} where Mössbauer spectroscopy showed tetrahedrally coordinated Fe^{3+}
– the remaining Al and Fe^{3+} together with Fe^{2+} were assigned to the octahedral sheet

Table 2. Mineral compositions of the samples (WR and <2 μm fractions) determined by XRD.

Sample	smectite	kaolinite	illite	plagioclase	quartz	opal-CT	calcite	zeolite	volcanic glass
BU	+ X			+	+	+ X	+		
ZG	+ X	+ X			+			+	+ X
BD	+ X	+ X		+	+	+	+ X	+	
DR	+ X		+ X	+	+ X				
ŠI1	+ X	+ X			+ X		+		
ŠI2	+ X	+ X			+ X		+		
SJ	+ X	+ X			+				
PR	+ X	+ X		+	+				
DI1	+ X	+ X							+
DI2	+ X	+ X		+	+				+ X
LV	+ X				+				
VB	+ X		+		+	+ X	+		
PL	+ X			+	+	+ X			

\+ present in the WR sample
X present in the < 2 μm fraction

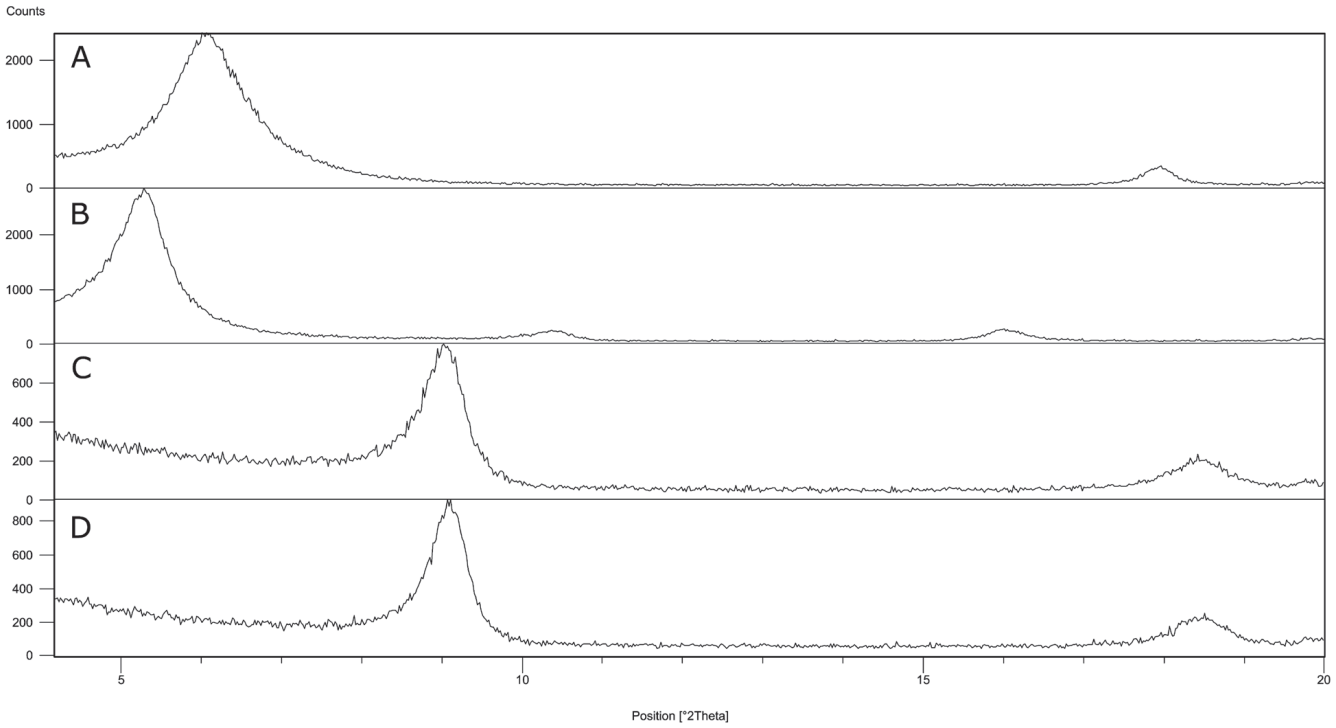

Figure 2. XRD patterns of BU <2 μm fraction, oriented samples, (A) air dried, (B) glycolated, (C) heated to 400 °C, (D) heated to 550 °C CuK$_\alpha$ radiation.

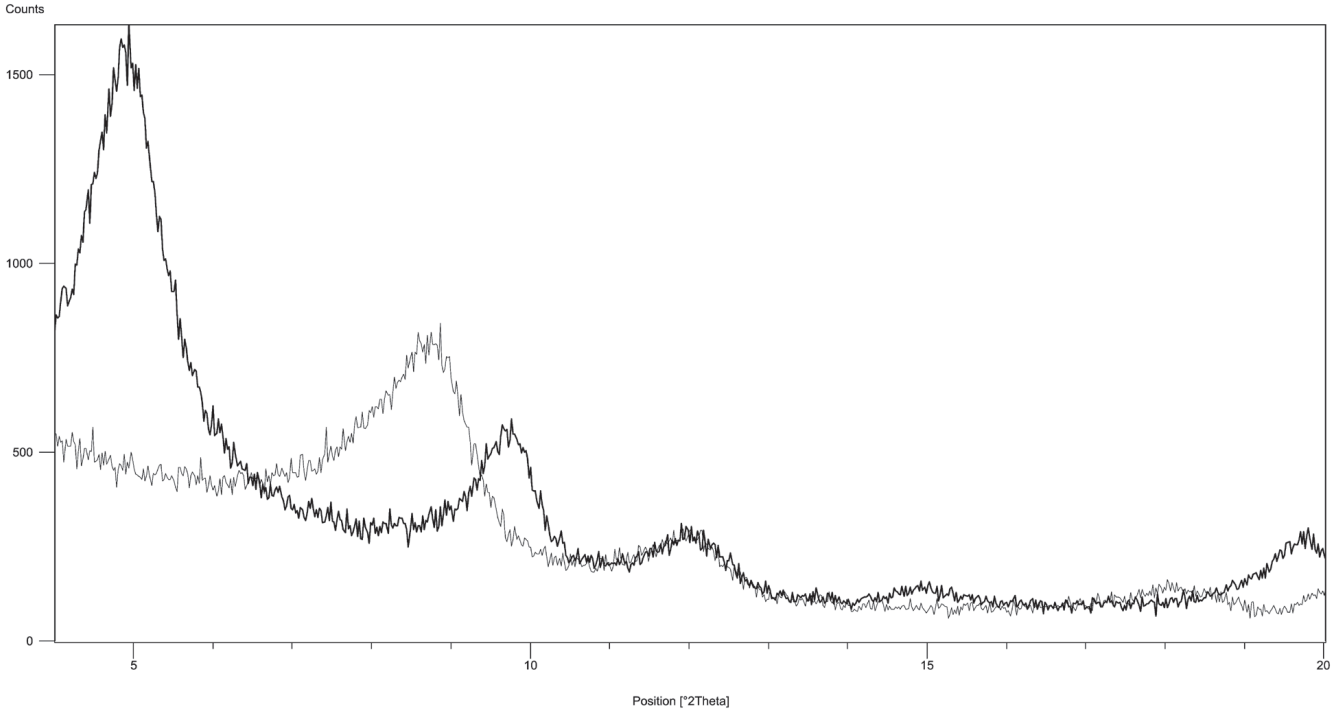

Figure 3. XRD patterns of DI1 sample (<2 μm) after Greene-Kelly test, lithium saturated sample heated at 200 °C (grey); after glycerol treatment (black) CuK$_\alpha$ radiation.

– the unoccupied spaces in the octahedral sheet were filled by Mg
– Na, Ca, K and leftover Mg were assigned to the interlayer.

3.6. Mössbauer spectroscopy

Fe distribution among the tetrahedral and octahedral sheets and its valence state was analysed using Mössbauer spectroscopy. Mössbauer spectra were recorded at room temperature using a constant acceleration Wissel spectrometer, in transmission mode with Co-57 source in Rh matrix. Velocity calibration was performed using a thin α-Fe foil. The isomer shifts are expressed relative to α-Fe at room temperature. The spectra were fitted with the analysis code RECOIL (LAGAREC & RANCOURT, 1998) using quadrupole doublets of Lorentzian lineshape.

4. RESULTS

4.1. X-ray diffraction (XRD)

Randomly oriented powder mounts of WR samples revealed that, apart from clay minerals, the samples contain variable amounts of other minerals: quartz, opal-CT, calcite, plagioclase feldspars

Table 3. *d*-values [Å] of 00*l* and 060 peaks measured on oriented sample (except for 060) of differently treated <2 μm fraction, and CV values for EG treated K-saturated samples.

	BU						ZG						BD					
	AD	EG	550 °C	Li-200-Gly	Mg-Gly	K-EG	AD	EG	550 °C	Li-200-Gly	Mg-Gly	K-EG	AD	EG	550 °C	Li-200-Gly	Mg-Gly	K-EG
001	14.50	16.78	9.80	9.70	18.07	14.12	14.56	17.38	9.69 (b)	9.41	18.06	16.36	10.66	17.15	9.85	9.60	18.09	15.70
002		8.546	4.812	4.756	9.06			8.286			8.357	8.86 (b)	4.868	8.72	4.822	4.7173	9.03	
003	4.947	5.528		3.2012	5.919	4.629		5.673			5.975	5.56 (b)	3.1957	5.60		3.20 (b, a)		
004					4.484	3.3974		4.43						4.32				
005	2.9931	3.3406		1.9293	3.5528			3.4282				3.461	1.9392	3.37		1.9331		3.3951
006		2.7800			2.9900	2.8428						2.829 (b)		2.82				2.8257
CV						2.72						2.96						4.40
060*	1.4983						1.4952						1.5023					

	DR						ŠI1						ŠI2					
	AD	EG	550 °C	Li-200-Gly	Mg-Gly	K-EG	AD	EG	550 °C	Li-200-Gly	Mg-Gly	K-EG	AD	EG	550 °C	Li-200-Gly	Mg-Gly	K-EG
001	12.49	17.20	9.84	9.71	18.10	16.40	14.32	17.32	10.11	17.60	18.47	14.23	15.09	17.15	9.67	9.65	18.16	15.77
002	4.934	8.586	4.814	4.745	9.08 (b)	8.93 (b)		8.443	4.889	9.13	9.14			8.518	4.744	4.774	9.023	
003		5.620		3.1504	5.95(b)	5.59 (b)	4.903	5.611		5.847	5.888	4,67 (b)	4.98	5.623			5.947	
004	3.1150	4.278					3.565	4.233		4.551	4.439	3.426						
005		3.3629		1.9302		3.417	2.993	3.3644		3.5088	3.588	2.779 (b)	3.00	3.3702				3.4180
006		2.8311						2.7905		3.0295	3.002			2.8162				2.824 (b)
CV						3.62						1.54						5.69
060*	1.4991						1.4983						1.4968					

	SJ						PR						DI1					
	AD	EG	550 °C	Li-200-Gly	Mg-Gly	K-EG	AD	EG	550 °C	Li-200-Gly	Mg-Gly	K-EG	AD	EG	550 °C	Li-200-Gly	Mg-Gly	K-EG
001	14.88	17.28	9.59	18.8	14.07 (17.56)	16.74	14.61	17.15	9.91	9.68	17.84 (14.24)	17.26	13.61	17.03	9.70	17.92	18.25	16.68
002	7.195	8.533	4.749	9.56	7.13(b)	8.686		8.533	4.819	4.744	8.921	8.659	7.410	8.470	4.78	9.119		8.893
003	5.008	5.657			4.735	5.712	4.944	5.661			5.929	5.738		5.620		5.938		5.623
004	3.5903	4.247		4.702		4.350		4.2575			4.749	4.3235	3.621			4.5002		
005	3.0300	3.3943				3.4251	3.0274	3.3961				3.4387	3.1518	3.3693		3.5556		3.4248
006		2.8324				2.8579		2.8318				2.8682		2.8114		3.0164		2.8490
CV						1.39						0.29						2.44
060*	1.4952						1.4975						1.4936					

	DI2						LV						VB					
	AD	EG	550 °C	Li-200-Gly	Mg-Gly	K-EG	AD	EG	550 °C	Li-200-Gly	Mg-Gly	K-EG	AD	EG	550 °C	Li-200-Gly	Mg-Gly	K-EG
001	15.22	17.46	10.00	18.07	18.57	17.27	15.05	17.33	10.15	9.70	18.59 (15.16)	16.20	12.9 (b, a)	17.13	9.77	17.85	18.06	17.26
002		8.621	4.849	9.16 (b)	9.055	8.648		8.588	4.827	4.758	9.162		6.176	8.521	4.825	9.357	8.975	8.683
003	5.047	5.659			6.013	5.658	4.966	5.651			6.001	5.667		5.657			5.955	5.724
004								4.289			4.817		3.1233	4.2454		4.606	4.476	4.3147
005		3.3932				3.4299	2.9886	3.3863				3.4079	2.4881	3.3907				3.4431
006		2.8194				2.8636		2.8251				2.8394		2.8298				2.8627
CV						0.74						2.47						0.42
060*	1.4975						1.4973						1.4967					

	PL					
	AD	EG	550 °C	Li-200-Gly	Mg-Gly	K-EG
001	14.95	17.02	9.84	9.68	17.82	17.04
002		8.496	4.762	4.705	8.943	8.716
003	4.990	5.636		3.18 (b, a)	5.926	5.682
004		4.222		2.50		
005	3.0225	3.3789		1.9361	3.5591	3.4223
006		2.8183			2.9688	2.8627
CV						0.94
060*	1.4975					

*Measured on randomly oriented samples
(values in parentheses indicate weaker peak)
b – broad
a- asymmetric

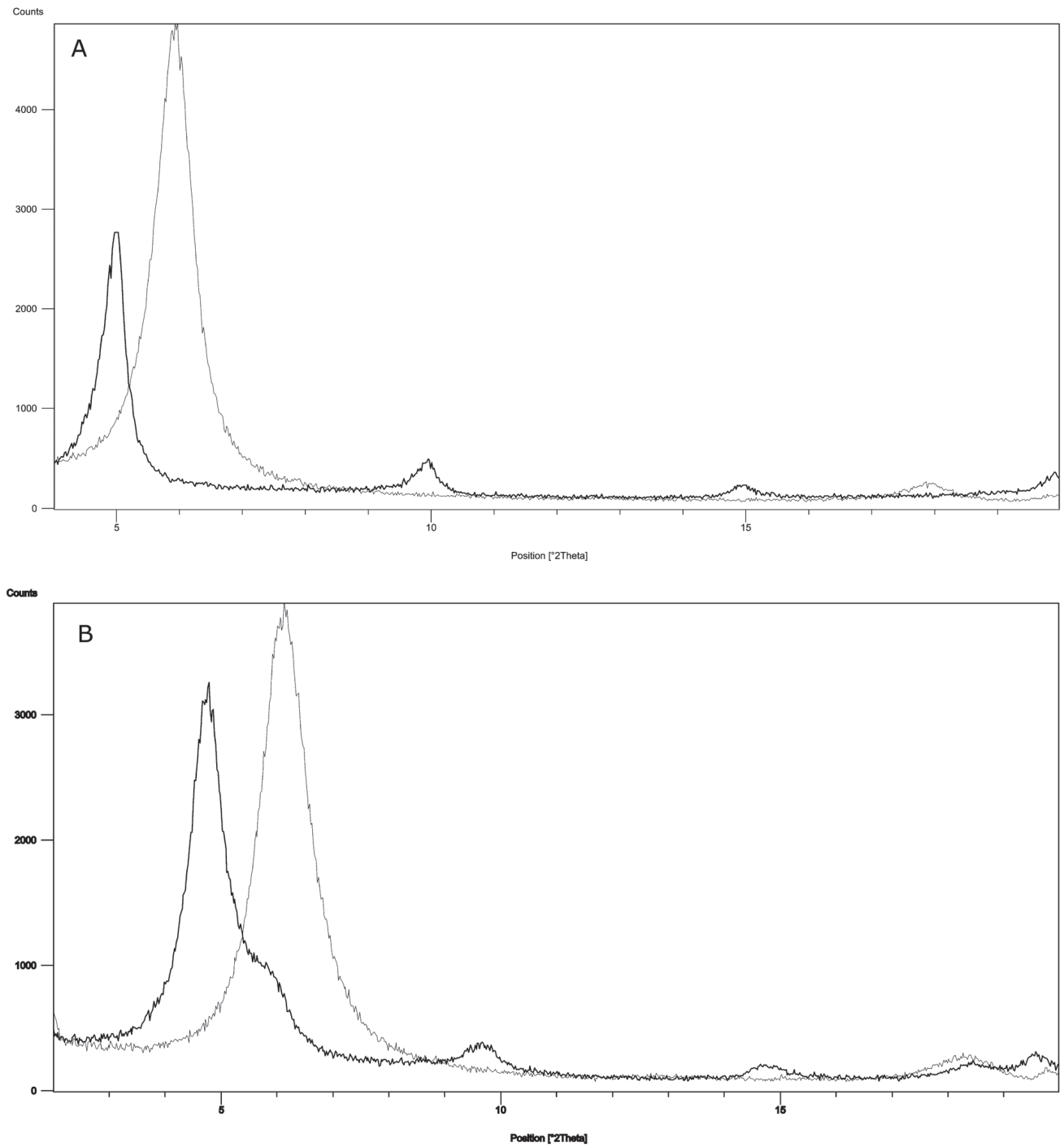

Figure 4. XRD patterns of <2 μm fraction of samples exchanged with Mg: (A) PL sample, before (grey) and after (black) glycerol solvation, showing behaviour typical for smectite and (B) LV sample showing the splitting of the 001 peak after the same treatment CuK_{α} radiation.

and zeolite from the heulandite-clinoptilolite series (Table 2). Opal-CT and quartz were also detected in the <2 μm fraction of some samples. Both randomly oriented powder samples and oriented clay-size mounts on glass slides showed that the main mineral in all of the samples is dioctahedral smectite ($d_{060} \approx 1.50$ Å) with small amounts of kaolinite present in some samples. Smectite was determined by a typical behaviour after EG treatment ($d_{001} \approx 17$ Å) and after heating at 400 and 550 °C ($d_{001} \approx 10$ Å) (Fig. 2, Table 3), while the first order kaolinite basal peak remained unchanged around 7 Å after EG treatment and heating to 400 °C, collapsing after heating to 550 °C. A couple of samples showed the presence of an amorphous substance (presumed to be volcanic glass), visible as a "hump" between and 20 and 30 °2Θ, on both randomly oriented and oriented mounts.

The Greene-Kelly test revealed the presence of beidellite in samples DI1 (Fig. 3), DI2 and ŠI1. After prolonged treatment with glycerol, an additional shift to 18 Å was observed for the VB and SJ samples. Mg-test confirmed the main mineral to be montmorillonite in most of the samples (Fig. 4A). Some samples (LV, PR and SJ) showed two peaks after glycerol treatment, one between 17 and 18 Å and a smaller one (more prominent only in the case of the SJ sample) around 14 Å (Fig. 4B, Table 3).

Samples saturated with K and treated with EG showed either full expansion to about 17 Å, negligible expansion with the 001

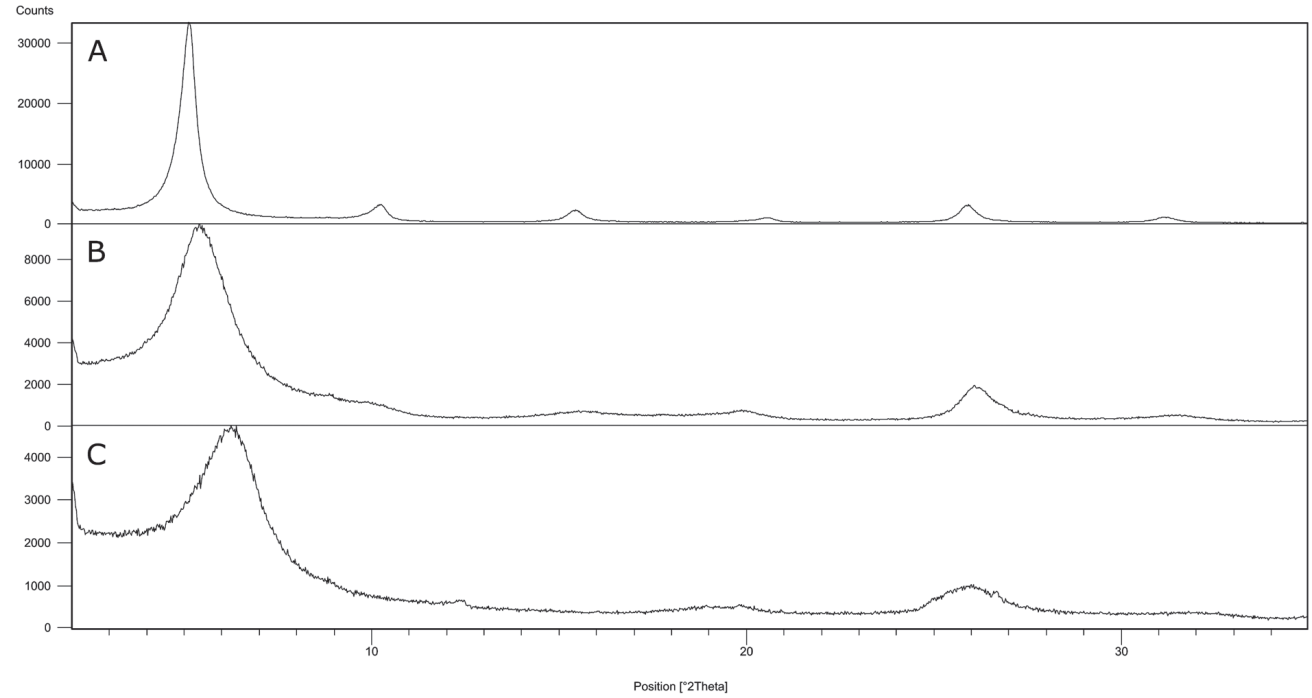

Figure 5. Comparison of XRD patterns of (A) low- (PR), (B) medium- (LV), and (C) high-charged (ŠI1) smectites after K saturation and EG treatment of <2 μm fraction CuK_α radiation.

peak remaining around 14 Å, or exhibited in-between values (Table 3, Fig 5).

Observed d_{060} values were in the range of values for montmorillonite: 1.492 – 1.504 Å (MOORE & REYNOLDS, 1997) (Table 3).

4.2. Fourier Transform Infrared (FTIR) spectroscopy

Results of the FTIR analysis of the clay-size fraction (Table 4) are in accordance with the XRD results. A well-defined 3700 cm^{-1} band, as well as the 795 and 753 cm^{-1} doublet (Fig. 6) confirm the presence of kaolinite in some samples. The spectra also allowed

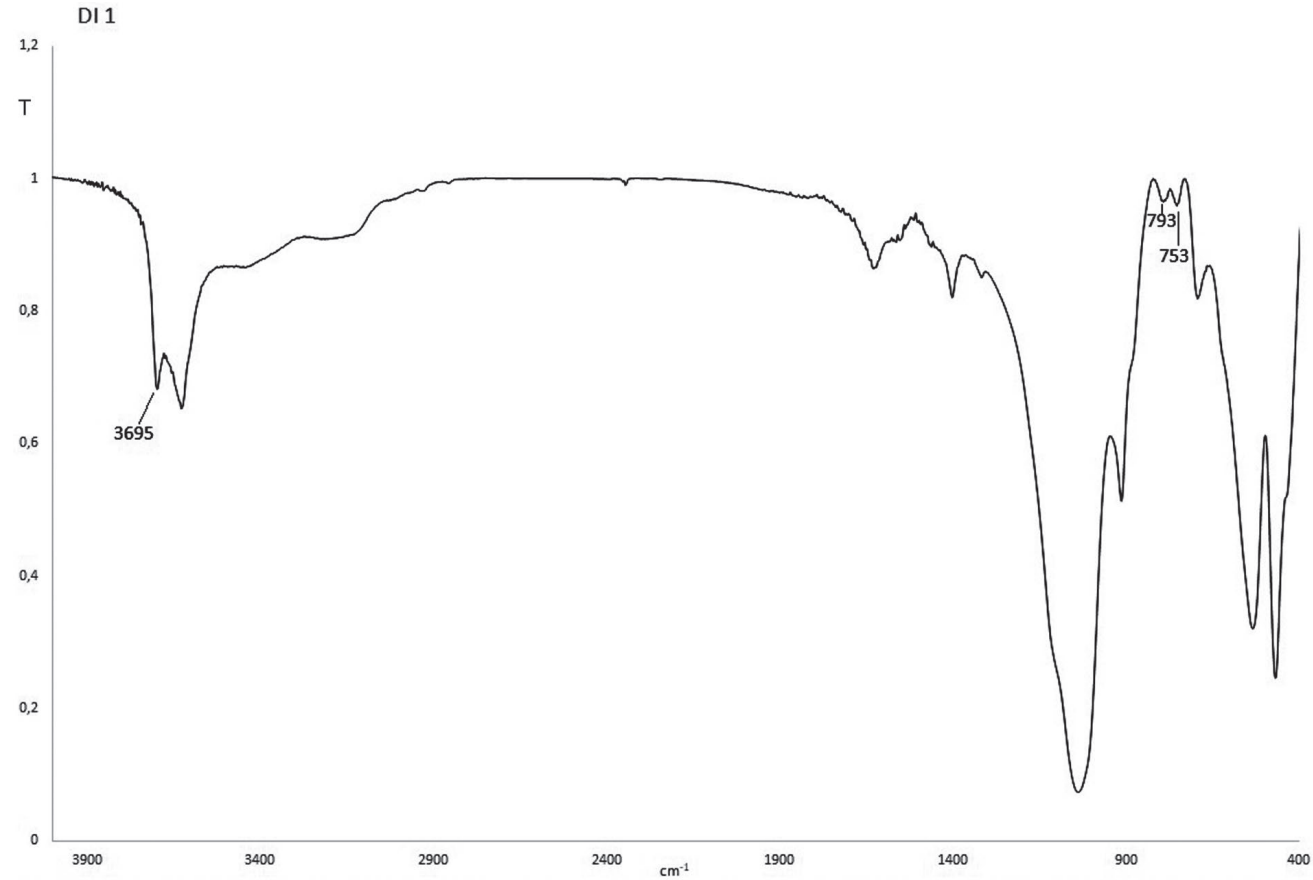

Figure 6. FTIR spectrum of DI1 (<2 μm) sample with wave numbers of bands showing presence of kaolinite.

Table 4. Assignments of FTIR bands observed in the <2 μm fractions of bentonites (after MADEJOVÁ & KOMADEL, 2001). Mnt – montmorillonite, Kln – kaolinite

Wavenumbers [cm^{-1}]													Assignement
BU	ZG	BD	DR	ŠI1	ŠI2	SJ	PR	DI1	DI2	LV	VB	PL	
	3704							3695					OH stretching of inner-surface hydroxyl groups (Kln)
3625	3628	3627	3629	3629	3625	3628	3632	3626	3628	3630	3634	3628	OH stretching of structural hydroxyl groups (Mnt)
1630	1630	1631	1631	1632	1627	1622	1629	1626	1627	1631	1622	1627	OH deformation of water
				1400	1402		1403	1402		weak 1401		1402	NH_4 deformation of NH_4Br
									1384				
						1316							
1089	-	-	-	-	-	-	-	-	-	-	broad	broad	Si-O stretching of cristobalite
1030	1039	1027	1035	1036	1037	1037	1048	1038	1047	1039	1044	1039	Si – O stretching
913	913	inflection	915	912	915	918	920	912	918	916	916	916	AlAlOH deformation (Mnt)
		inflection 880				inflection 889	884		inflection 884		inflection 885		AlFeOH deformation (Mnt)
843	842	inflection 843	838		845	inflection 847	852			845	inflection 849		AlMgOH deformation (Mnt)
		weak 800	weak 800				802					808	Si-O stretching of quartz and silica
795					795				795	798	797	795	Si-O stretching of cristobalite
	798							793					Si – O (Kln)
						782							
	753							753					Si – O perpendicular (Kln)
				697				692					Si-O, perpendicular
625					627	626	624			626	624	626	Coupled Al-O and Si-O, out-of-plane; Si-O of cristobalite
	607												
520	529	523	520	527	522	525	525	533	525	522	525	521	Al – O – Si deformation (Mnt)
466	472	470	470	468	467	470	468	469	467	467	469	467	Si – O – Si deformation (Mnt)
		430		424									Si – O deformation

a more detailed definition of some structural properties, e.g. cations in the octahedral coordination.

The type of octahedrally coordinated cations present in the smectite structure is visible from AlAlOH (915 cm^{-1}), AlMgOH (840 cm^{-1}) and AlFeOH (885 cm^{-1}) deformation bands (MADEJOVÁ & KOMADEL, 2001) (Fig. 7). All samples showed the AlAlOH band, while the presence of the AlMgOH and AlFeOH bands varied (Table 4).

A broad band around 3420 cm^{-1} representing the OH stretching of water is visible on all spectra. After heating the KBr pellets, its intensity diminished, however its complete disappearance was not achieved.

4.3. CEC determination

CEC of the samples varied between 44 and 94 cmol(+)/kg with one sample from Divoselo (DI2) showing an anomalously low value of 19 cmol(+)/kg (Table 5).

4.4. Thermal analyses

All of the samples show a single or double endothermic peak assigned to the dehydration process between 100 and 200 °C, as well as one or more endothermic peaks at higher temperatures, between 450 and 700 °C assigned to dehydroxylation (Table 6). Some samples show exothermic peaks around 450 °C indicating organic matter oxidation and/or above 900 °C due to recrystallization (Fig. 8).

4.5. Chemical analysis

The chemical composition of WR and of the <2 μm fraction of the samples is shown in Tables 7 and 8. Data for the <2 μm fraction were used to calculate the chemical formula of smectite (Table 9), while the WR chemistry, specifically the concentration of immobile elements, was used to deduce the composition of parent (volcanic) material.

4.6. Mössbauer spectroscopy

Mössbauer spectra recorded at room temperature differ significantly between samples (Fig. 9, Table 10). Some of them (BU and ŠI1) could be fitted with a single doublet characteristic for Fe^{3+} in the octahedral coordination, while others had to be fitted with more doublets. Spectra of ŠI2 and DI1 were fitted with two doublets for Fe^{3+} in the octahedral coordination, while for the rest of the samples (except BD) one additional doublet attributed to Fe^{2+} in octahedral coordination had to be used. For the BD sample, the fit was made with four doublets, three previously mentioned and an additional one for Fe^{3+} in tetrahedral coordination. Assignment to different Fe species was made in accordance with BARON et al. (2017), PELAYO et al. (2018) and references therein. There is no clear evidence of the presence of a magnetically ordered phase, which indicates that most of the Fe present in the fine fraction of the investigated smectites is incorporated into the smectite structure.

5. DISCUSSION

5.1. Mineral and parent material composition

The mineral composition of both the WR and clay-size fractions show the samples vary between almost monomineralic to polymineralic containing a number of

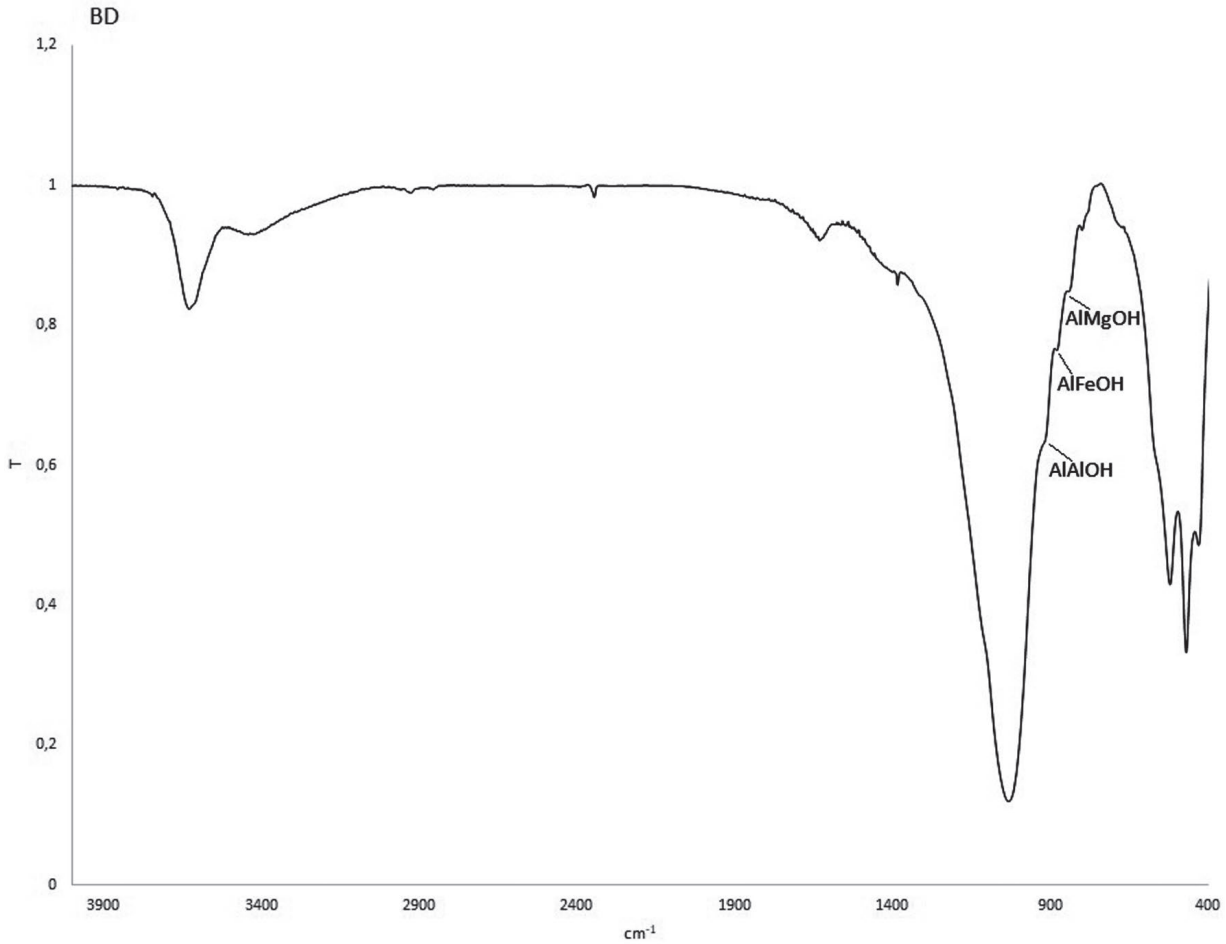

Figure 7. FTIR spectrum of BD (<2 μm) sample with bands characteristic of the different octahedral cations indicated.

Table 5. Measured CEC values (WR samples)

Sample	CEC [cmol(+)/kg]
BU	60
ZG	60
BD	85
DR	94
ŠI1	82
ŠI2	91
SJ	78
PR	53
DI1	64
DI2	19
LV	85
VB	44
PL	72

additional minerals (Table 2). Smectite is the dominant mineral in the <2 μm fraction. Kaolinite is present in 8 samples, and some silica minerals (quartz and/or opal-CT) remained in the <2 μm fraction after separation. The most problematic for further analyses was the presence of amorphous impurities (most likely volcanic glass) in samples ZG, DI1 and DI2.

The Greene-Kelly test showed the majority of samples contain montmorillonite and only some (DI1, DI2 and ŠI1) could unambiguously be classified as beidellite following their expansion after lithium saturation and glycerol treatment. For the other samples (SJ, PR and VB) that showed swelling after the Greene-Kelly test, other analyses were not conclusive for the presence of beidellite.

The Mg-test was even less conclusive and showed some samples (SJ, PR and LV) retained (almost completely or partially) the 14 Å peak position after glycerol treatment, even when other analyses showed that their layer charge was not high enough for vermiculite. This could be due to incomplete glycerol saturation, or the presence of interstratification of differently charged layers which was confirmed by the irrational order of the 00*l* series.

The determined mineral composition of the samples is in overall good correlation with the existing literature data

Table 6. Observed temperatures of thermal reactions measured on <2 μm fractions of bentonites.

Sample	Dehydration temperature [°C]	Dehydroxylation temperature [°C]
BU	105 + shoulder at 165	660
ZG	125 + shoulder at 180	510 + weaker broad peak at 620
BD	110	broad peak below 600 + shoulder at 680
DR	105	peak at 635 + weaker broad peak at 480
ŠI1	110 + shoulder 180	485
ŠI2	135 + shoulder at 180	670
SJ	125 + shoulder at 175	broad 670 + weak broad at 520
PR	120 + shoulder at 160	680
DI1	100 + shoulder at 150	470 and a weak broad peak at 670
DI2	110 + shoulder at 165	650
LV	120 + shoulder at 170	670
VB	120 + shoulder at 160	asymmetric peak at 670 with a shoulder at 610
PL	100 + shoulder at 155	660

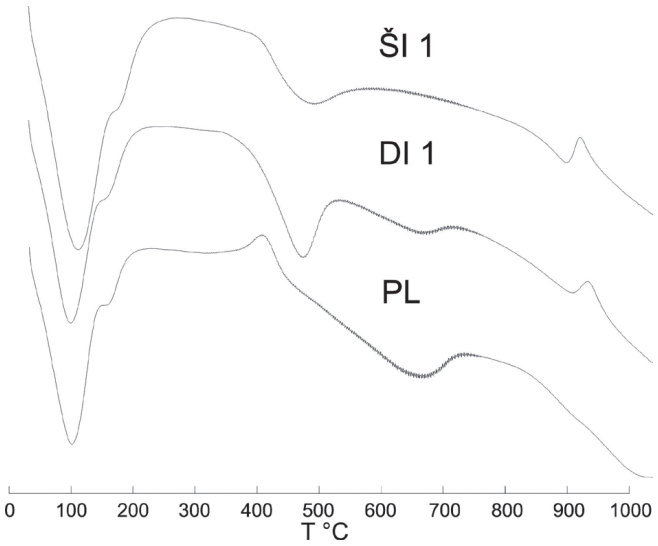

Figure 8. DTA curves of three representative samples, ŠI1, DI1 and PL (<2 μm fractions) differing in dehydroxylation temperature range. In addition to endothermic peaks due to dehydration and dehyroxilation PL sample shows exothermal peak caused by organic matter oxidation while peaks due to recrystallization are visible on ŠI1 and DI1 DTA curves.

(BRAUN, 1991; MARKOVIĆ, 2002; MILADINOVIĆ, 1976; VUJNOVIĆ, 1981), with the exception of beidellite found in samples from Divoselo.

FTIR spectra provided more information on dioctahedral smectite in the samples and confirmed the presence of some mineral impurities (Table 4). Kaolinite was confirmed in samples ZG and DI1; however, it was not confirmed in other samples where XRD indicated its presence. The 3700, 3620 cm^{-1} doublet is characteristic of the kaolin group, as well as OH deformation bands at 938 and 916 cm^{-1} (RUSSELL & FRASER, 1994). In the investigated samples, the 3620 cm^{-1} band was overshadowed by a broad stretching band of the structural hydroxyl group in smectites and 938 and 916 cm^{-1} bands are probably also covered by smectite bands. The ZG and DI1 samples also showed two small bands around 795 and 753 cm^{-1} of roughly equal intensity, characteristic for kaolinites (RUSSELL & FRASER, 1994). Silica impurities were also confirmed: a most notable band around 1090 cm^{-1} representing Si-O stretching of cristobalite in samples BU, VB and PL and 795 cm^{-1} in samples BU, ŠI2, DI2, LV, VB and PL. Quartz or silica, determined by a Si-O stretching band at 800 cm^{-1} was found in samples BD, DR, PR and PL.

Some discrepancy between the content of impurities shown between XRD and FTIR results could be the result of peak overlapping in recorded XRD patterns and FTIR spectra and/or the presence of impurities in concentrations below the detection limit. This demonstrates the benefits of using both methods to complement each other. Additionally, the thermal analysis showed an exothermal peak in the 450 °C region indicating possible presence of organic matter in some samples (BU, BD and PL) which have the highest TOT/C.

The mineral composition of the samples is the result of the parent material chemical composition. With that in mind, immobile element (Ti, Zr, Nb and Y) content was used to determine parent material composition from the discrimination diagram after WINCHESTER & FLOYD (1977) (Fig. 10). This diagram shows that most samples originate from acidic to neutral volcanoclastic material, with sample BD standing out as andesitic in composition. This can explain the highest Fe content in the BD

Table 7. Chemical composition of WR samples.

Analyte	Unit	MDL	BU WR	ZG WR	BD WR	DR WR	ŠI1 WR	ŠI2 WR	SJ WR	PR WR	DI1 WR	DI2 WR	LV WR	VB WR	PL WR
SiO_2	%	0.01	63.66	49.80	53.75	53.44	45.55	51.31	51.42	52.99	45.12	64.61	52.59	65.18	63.19
Al_2O_3	%	0.01	11.01	21.13	14.03	15.28	18.28	17.31	19.85	18.36	25.78	14.27	16.77	13.47	12.46
Fe_2O_3	%	0.04	0.73	2.54	5.93	3.15	4.35	1.97	2.78	4.08	4.4	2.41	2.36	2.24	1.7
MgO	%	0.01	2.78	3.05	4.15	4.48	2.25	3.58	2.43	2.48	0.77	0.70	3.62	1.95	2.27
CaO	%	0.01	4.58	0.97	1.4	1.52	5.62	2.44	2.29	2.87	1.63	1.40	1.93	1.70	2.36
Na_2O	%	0.01	0.24	0.01	1.75	1.01	0.02	0.04	0.05	0.61	0.05	1.74	0.20	0.67	0.31
K_2O	%	0.01	1.28	0.11	0.88	0.41	0.26	0.20	0.39	0.20	0.12	3.48	0.53	0.78	0.35
TiO_2	%	0.01	0.11	0.27	0.63	0.11	0.53	0.25	0.29	0.26	0.22	0.13	0.20	0.21	0.09
P_2O_5	%	0.01	0.02	<0.01	0.07	0.02	0.01	0.05	0.09	0.11	0.04	0.01	0.07	0.05	0.02
MnO	%	0.01	<0.01	<0.01	0.02	0.01	0.03	<0.01	0.01	0.01	0.04	0.05	<0.01	0.04	<0,01
Cr_2O_3	%	0.002	0.004	<0.002	0.004	0.002	0.008	<0.002	<0.002	<0.002	0.003	<0.002	<0.002	0.003	0.008
Ba	ppm	5	173	46	153	402	807	298	138	141	1158	617	266	169	221
Ni	ppm	20	30	<20	21	<20	28	<20	<20	<20	<20	<20	<20	<20	35
Sr	ppm	2	56	60	350	240	166	30	40	126	21	44	118	312	158
Zr	ppm	5	88	208	191	105	242	161	134	167	417	239	280	90	138
Y	ppm	3	20	18	38	23	18	10	7	10	41	36	26	13	18
Nb	ppm	5	16	13	6	11	17	17	11	9	33	19	27	12.3	12
Sc	ppm	1	3	6	14	5	12	5	4	4	20	11	4	4	7
LOI	%	-5.1	15.5	22.0	17.2	20.4	22.9	22.7	20.3	17.9	21.6	11.0	21.5	13.6	17.1
Sum	%	0.01	99.95	99.90	99.92	99.91	99.93	99.86	99.89	99.87	99.95	99.86	99.83	99.88	99.96
TOT/C	%	0.02	0.71	0.04	0.31	0.19	0.98	<0.02	0.05	0.18	0.09	0.02	0.02	0.11	0.24
TOT/S	%	0.02	<0.02	<0.02	<0.02	<0.02	<0.02	<0.02	<0.02	0.02	<0.02	<0.02	<0.02	<0.02	<0.02

MDL - method detection limit

Table 8. Chemical composition of <2 μm fraction.

Analyte	Unit	MDL	BU <2 μm	ZG <2 μm	BD <2 μm	DR <2 μm	ŠI1 <2 μm	ŠI2 <2 μm	SJ <2 μm	PR <2 μm	DI1 <2 μm	DI2 <2 μm	LV <2 μm	VB <2 μm	PL <2 μm
SiO_2	%	0.01	60.55	50.17	51.13	53.26	46.77	50.07	50.22	52.88	45.2	52.51	51.53	62.25	63.26
Al_2O_3	%	0.01	13.28	22.18	13.85	15.91	20.47	17.28	19.78	17.62	24.56	17.49	16.84	14.78	12.33
Fe_2O_3*	%	0.04	1.41	2.47	5.61	3.58	4.99	2.28	2.37	3.55	4.68	3.86	2.27	2.17	1.58
FeO*	%	-	0.00	0.11	0.91	0.47	0.00	0.00	0.14	0.28	0.00	0.32	0.32	0.12	0.07
MgO	%	0.01	3.86	2.98	4.23	4.03	2.55	3.59	2.38	2.57	0.89	1.94	3.84	2.19	2.35
CaO	%	0.01	2.29	0.97	1.33	1.36	1.66	2.56	2.49	2.26	1.71	2.53	1.96	2.00	2.39
Na_2O	%	0.01	0.10	0.07	2.74	1.25	0.01	0.06	0.08	0.09	0.09	0.27	0.12	1.09	0.17
K_2O	%	0.01	1.09	0.11	0.50	0.80	0.24	0.17	0.16	0.07	0.15	0.62	0.31	0.22	0.20
TiO_2	%	0.01	0.12	0.25	0.64	0.20	0.42	0.25	0.18	0.14	0.18	0.16	0.18	0.08	0.08
P_2O_5	%	0.01	<0.01	<0.01	0.06	0.07	0.02	<0.01	<0.01	<0.01	0.02	<0.01	0.02	<0.01	<0,01
MnO	%	0.01	<0.01	<0.01	0.02	0.02	0.02	<0.01	<0.01	<0.01	0.03	0.05	<0.01	0.02	<0,01
Cr_2O_3	%	0.002	0.006	<0,002	0.004	0.011	0.009	<0,002	<0,002	<0,002	<0,002	<0,002	<0,002	<0,002	<0,002
Ba	ppm	5	72	50	264	328	154	62	64	67	1092	176	103	24	160
Ni	ppm	20	62	<20	<20	31	32	<20	<20	<20	21	<20	<20	<20	<20
Sr	ppm	2	28	59	251	183	155	28	35	78	24	22	118	269	152
Zr	ppm	5	81	232	202	97	165	99	57	84	270	234	208	68	103
Y	ppm	3	19	20	34	21	15	9	5	8	32	27	23	7	13
Nb	ppm	5	21	13	6	12	17	16	7	7	14	25	29	9	10
LOI**	%	-5.1	17.2	20.6	18.6	18.8	22.7	23.6	22.1	20.4	22.3	20.1	22.4	15.0	17.5
Sum	%	0.01	99.92	99.89	99.91	99.92	99.93	99.90	99.93	99.91	99.93	99.87	99.85	99.90	99.96
TOT/C	%	0.02	0.25	0.14	0.44	0.24	0.15	0.05	0.13	0.19	0.14	0.25	0.08	0.35	0.40
TOT/S	%	0.02	<0.02	<0.02	<0.02	<0.02	<0.02	0.02	<0.02	<0.02	<0.02	<0.02	<0.02	0.06	<0.02

*values calculated according to Mössbauer spectra
**value corrected for FeO

Table 9. Calculated chemical formulae of investigated bentonite samples.

Samples		BU	ZG	BD	DR	ŠI1	ŠI2	SJ	PR	DI1	DI2	LV	VB	PL
Corrections		-25% opal-CT	-10% kaolinite	-1% calcite -1% kaolinite	-2% quartz	-1% quartz -1% kaolinite				-10% kaolinite			-20% opal-CT	-25% opal-CT
Tetrahedral	Cations	$Si_{3.72}$ $Al_{0.28}$	$Si_{3.80}$ $Al_{0.20}$	$Si_{3.91}$ $Fe^{3+}_{0.03}$ $Al_{0.06}$	$Si_{3.91}$ $Al_{0.09}$	$Si_{3.62}$ $Al_{0.38}$	$Si_{3.89}$ $Al_{0.11}$	$Si_{3.82}$ $Al_{0.18}$	$Si_{3.94}$ $Al_{0.06}$	$Si_{3.54}$ $Al_{0.46}$	$Si_{3.93}$ $Al_{0.07}$	$Si_{3.94}$ $Al_{0.06}$	$Si_{3.88}$ $Al_{0.12}$	$Si_{3.95}$ $Al_{0.05}$
	Charge (% of total layer charge)	-0.28 (35%)	-0.20 (43%)	-0.09 (15%)	-0.09 (17%)	-0.38 (67%)	-0.11 (22%)	-0.18 (40%)	-0.06 (16%)	-0.46 (94%)	-0.07 (23%)	-0.06 (13%)	-0.12 (28%)	-0.05 (12%)
Octahedral	Cations	$Al_{1.36}$ $Fe^{3+}_{0.11}$ $Mg_{0.53}$	$Al_{1.59}$ $Fe^{3+}_{0.15}$ $Fe^{2+}_{0.01}$ $Mg_{0.25}$	$Al_{1.17}$ $Fe^{3+}_{0.30}$ $Fe^{2+}_{0.06}$ $Mg_{0.47}$	$Al_{1.34}$ $Fe^{3+}_{0.21}$ $Fe^{2+}_{0.03}$ $Mg_{0.42}$	$Al_{1.51}$ $Fe^{3+}_{0.30}$ $Mg_{0.19}$	$Al_{1.47}$ $Fe^{3+}_{0.13}$ $Mg_{0.40}$	$Al_{1.59}$ $Fe^{3+}_{0.14}$ $Fe^{2+}_{0.01}$ $Mg_{0.26}$	$Al_{1.49}$ $Fe^{3+}_{0.20}$ $Fe^{2+}_{0.02}$ $Mg_{0.29}$	$Al_{1.66}$ $Fe^{3+}_{0.31}$ $Mg_{0.03}$	$Al_{1.47}$ $Fe^{3+}_{0.22}$ $Fe^{2+}_{0.02}$ $Mg_{0.22}$	$Al_{1.46}$ $Fe^{3+}_{0.13}$ $Fe^{2+}_{0.02}$ $Mg_{0.39}$	$Al_{1.48}$ $Fe^{3+}_{0.15}$ $Fe^{2+}_{0.01}$ $Mg_{0.30}$	$Al_{1.45}$ $Fe^{3+}_{0.12}$ $Fe^{2+}_{0.01}$ $Mg_{0.36}$
	Sum of octahedral cations	2.00	2.00	2.00	2.00	2.00	2.00	2.00	2.00	2.00	1.93	2.00	1.94	1.94
	Charge (% of total layer charge)	-0.53 (65%)	-0.26 (57%)	-0.53 (85%)	-0.45 (83%)	-0.19 (33%)	-0.40 (78%)	-0.27 (60%)	-0.31 (84%)	0.03 (6%)	-0.24 (77%)	-0.41 (87%)	-0.31 (72%)	-0.37 (88%)
Total layer charge (T+O)		-0.81	-0.46	-0.62	-0.54	-0.57	-0.51	-0.45	-0.37	-0.49	-0.31	-0.47	-0.43	-0.42
Interlayer	Cations	$Ca_{0.26}$ $Mg_{0.07}$ $Na_{0.02}$ $K_{0.15}$	$Ca_{0.09}$ $Mg_{0.12}$ $Na_{0.01}$ $K_{0.01}$	$Ca_{0.06}$ $Mg_{0.02}$ $Na_{0.41}$ $K_{0.05}$	$Ca_{0.11}$ $Mg_{0.04}$ $Na_{0.18}$ $K_{0.08}$	$Ca_{0.14}$ $Mg_{0.11}$ $K_{0.02}$	$Ca_{0.21}$ $Mg_{0.02}$ $Na_{0.01}$ $K_{0.02}$	$Ca_{0.20}$ $Mg_{0.01}$ $Na_{0.01}$ $K_{0.02}$	$Ca_{0.18}$ $Na_{0.01}$	$Ca_{0.16}$ $Mg_{0.09}$ $Na_{0.02}$ $K_{0.02}$	$Ca_{0.20}$ $Na_{0.04}$ $K_{0.06}$	$Ca_{0.16}$ $Mg_{0.05}$ $Na_{0.02}$ $K_{0.03}$	$Ca_{0.20}$ $Na_{0.19}$ $K_{0.03}$	$Ca_{0.26}$ $Na_{0.03}$ $K_{0.03}$
	Charge	+0.83	+0.44	+0.62	+0.56	+0.52	+0.49	+0.45	+0.37	+0.54	+0.50	+0.47	+0.62	+0.32

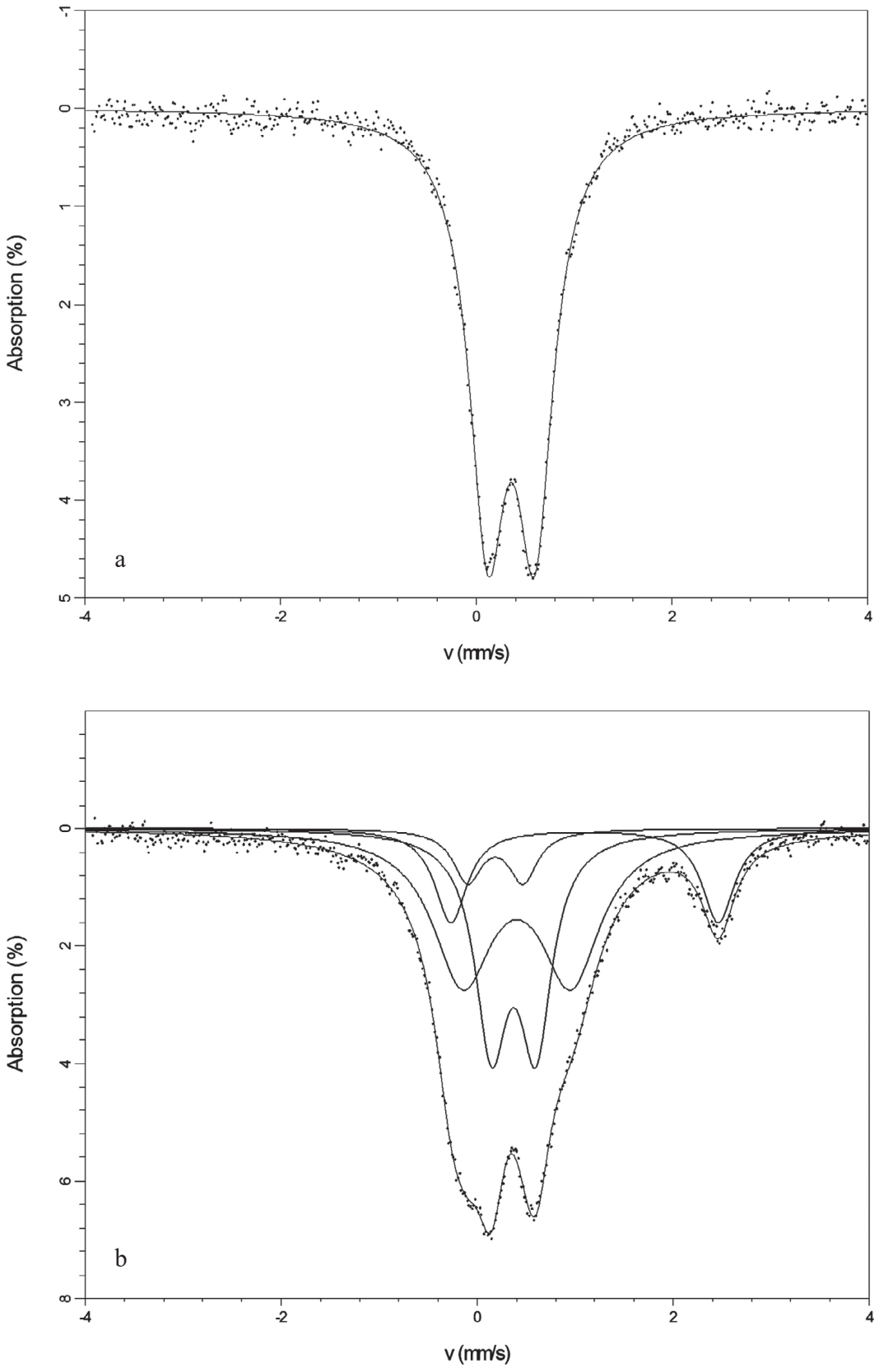

Figure 9. Mössbauer spectra of (a) BU and (b) BD samples (<2 μm) recorded at room temperature.

sample. The initial hypothesis that the samples containing beidellite, and thus less SiO_2, originate from more basic material was not confirmed. Still, in the case of altered pyroclastic rocks, elemental analyses should be taken cautiously as different materials could have been deposited in the same basin. Moreover, the volcanic material could have been separated during transport, especially in the case of distant depositional basins, which is mostly the case for the studied samples.

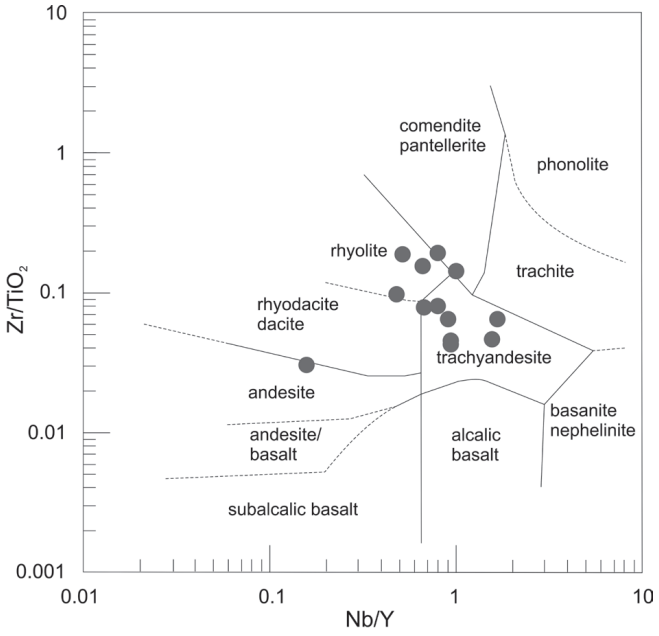

Figure 10. Content of immobile elements in analyzed bentonites plotted on the diagram for determination of original composition of altered rocks (WINCHESTER & FLOYD, 1977).

5.2. Crystallo-chemical properties of the investigated smectites and their classification

Some trends could be observed regarding the chemical composition of the investigated smectites (Tables 7 and 8): the main elements did not show large variation between WR and the <2 μm fraction with the exception of a much higher calcium concentration in WR of BU and ŠI1 samples, due to calcite presence. Among microelements, zirconium, usually present in zircon which is expected in the silt fraction, is more abundant in the WR, as well as strontium which can replace calcium in calcite and plagioclase. In contrast, the Ni and Fe concentrations showed negative correlation with particle size.

Structural chemical formulae calculated from the chemical composition of samples' <2 μm fractions could be compromised with crystalline and especially amorphous impurities present (BRIGATTI, 1983). Therefore, the resulting chemical formulae (Table 9) represent an approximate distribution of cations in the smectite structure. They can show some chemical and structural features of the smectite, such as layer charge, its distribution and the chemical composition of the octahedral sheet. Nevertheless, additional analyses were used to confirm (or disprove) these. Some calculated formulae show inconsistencies, e.g. charge imbalance or divergence from the results of other analyses. For example, the calculated layer charge for BU and, to lesser extent, for BD samples is too high for smectites, yet the Mg-test did not show the presence of vermiculite in those samples. Samples DI2 and VB have a significant discrepancy between their calculated layer charge and the interlayer cations compensating for it, which could be explained by the presence of amorphous impurities in the DI2 sample, but remains speculative in the case of the VB sample.

According to the chemical composition, the dominant cation in the interlayer is Ca for most samples, except BD and DR where Na is more abundant and VB in which both cations are equally represented. In the ZG sample, the calculated structural formula would suggest Mg is the dominant interlayer cation; however we cannot be sure of the accuracy of the formula due to amorphous impurities detected in this sample, it is probably more likely Ca as well (DRŽAJ & LUKACS, 1968).

There are a number of smectite classification schemes in the existing literature (GRIM & KULBICKI, 1961; SCHULTZ, 1969; BRIGATTI & POPPI, 1981) taking into account different criteria, such as layer charge, chemical composition and structure.

EMMERICH et al. (2009) with the general composition Mx+(Si4-yAly proposed a new classification scheme, in order to account for many discrepancies between known samples of bentonites not fitting into historical classification criteria, based on the following groups of analytical data:

– layer charge,
– structure of the octahedral sheet,
– iron content, and
– charge location.

These four criteria were used to further describe the smectite in the investigated bentonites.

Table 10. Mössbauer parameters obtained from the fit of the Mössbauer spectra recorded at room temperature on the studied smectites [mm/s], assignment to different Fe-species and their relative concentrations. Width is expressed as half width at half maximum (HWHM), isomer shift is specified relative to α-Fe.

	Fe^{3+} (VI) (A)				Fe^{3+} (VI) (B)				Fe^{2+} (VI)				Fe^{3+} (IV)			
	δ	Δ	width	area	δ	Δ	width	area	δ	Δ	width	area	δ	Δ	width	area
Sample	[mm/s]	[mm/s]	[mm/s]	[%]	[mm/s]	[mm/s]	[mm/s]	[%]	[mm/s]	[mm/s]	[mm/s]	[%]	[mm/s]	[mm/s]	[mm/s]	[%]
BU	0.35	0.48	0.23	100.0	-	-	-	-	-	-	-	-	-	-	-	-
ZG	0.36	0.53	0.25	61.0	0.36	1.00	0.48	35.0	1.06	2.69	0.42	4.8	-	-	-	-
BD	0.37	0.45	0.20	33.3	0.40	1.10	0.37	44.1	1.10	2.73	0.20	15.3	0.19	0.57	0.18	7.4
DR	0.35	0.43	0.26	63.4	0.39	1.24	0.30	23.9	1.13	2.66	0.22	12.7	-	-	-	-
ŠI1	0.36	0.50	0.27	100.0	-	-	-	-	-	-	-	-	-	-	-	-
ŠI2	0.36	0.52	0.17	52.0	0.36	0.87	0.38	48.0	-	-	-	-	-	-	-	-
SJ	0.36	0.52	0.20	58.0	0.38	1.08	0.36	36.0	1.11	2.57	0.30	6.0	-	-	-	-
PR	0.34	0.68	0.33	88.2	0.67	1.11	0.13	3.8	0.97	2.81	0.37	8.0	-	-	-	-
DI1	0.35	0.51	0.22	72.0	0.39	0.96	0.39	28.0	-	-	-	-	-	-	-	-
DI2	0.35	0.54	0.22	68.3	0.45	1.19	0.33	23.2	0.99	2.68	0.37	8.5	-	-	-	-
LV	0.35	0.43	0.23	50.0	0.38	1.11	0.39	36.0	1.16	2.82	0.22	13.5	-	-	-	-
VB	0.33	0.46	0.28	49.0	0.41	0.94	0.51	45.0	1.12	2.82	0.18	5.9	-	-	-	-
PL	0.35	0.58	0.26	48.0	0.36	1.09	0.44	47.0	1.30	2.40	0.14	4.9	-	-	-	-

S – broad peak with shoulder

According to EMMERICH et al. (2009) the interlayer cations are not considered for classification, nevertheless the descriptive name can be extended with respect to the original or exchanged interlayer cations, which, on one hand indicate conditions during smectite formation, and on the other, are responsible for its properties.

5.2.1. Layer charge

The layer charge was determined using both calculated and observed data, bearing in mind that chemical formulae calculations are affected by the presence of impurities in the samples. The layer charge from the calculated chemical formulae showed most samples are in the medium charge range, with values 0.31-0.54 per formula unit (FU) or half unit cell, with a few exceptions: ŠI1 (0,57), BD (0,62), and especially BU (0,81). Smectites are defined as 2:1 phyllosilicates with expandable layers and a layer charge between approximately 0.2 and 0.6/FU (GUGGENHEIM et al., 2006); therefore, BU would not satisfy that criteria. However, due to the already mentioned difficulties in obtaining an accurate chemical formula, and thus a calculated layer charge, the emphasis is put on the swelling behaviour of Mg-saturated samples treated with glycerol when it comes to differentiation between smectites and vermiculites. All of the investigated samples (in Mg-form), except SJ and partly PR and LV swelled after glycerol solvation, even if for some of them (BD and BU were not among them) a longer time was necessary for full swelling. The SJ sample, which is medium charged according to both its chemical formula and swelling behaviour of K-saturated form, showed splitting of the 001 peak: only a small portion of the peak moved to 17.6 Å while the majority remained at 14.0 Å.

Samples saturated with K and treated with EG showed either full expansion to about 17 Å, negligible expansion (001 peak remaining around 14 Å) or showed in-between values. Accordingly, based on the layer charge inferred from such swelling behaviours samples can be divided into three groups: those with low layer charge expanding fully, those with high layer charge (non-expanding) and the samples showing in-between values and an irrational series of 00*l* peaks. Coefficient of variation (CV) of d_{00l} values for K-saturated samples analysed after EG treatment were used to determine the stacking order of the clay mineral layers. Fully expandable samples, i.e. those with low-charge layers (PR, VB, DI2 and PL) exhibit a rational order of basal peaks and have a CV below or slightly above 0.75% (value defined by BAILEY, 1982) indicating periodic stacking of layers. Samples with expansion behaviour that suggests their layers are medium- to high-charged show an irrational order of basal peaks and higher CV values (Table 3). ČÍČEL & MACHAJDÍK (1981) investigated the three types of layers (expandable, partly expandable and non-expandable) in smectites saturated with monovalent ions with low solvation energy and concluded they are most commonly randomly distributed in the minerals. Likewise, the overall conclusion drawn about the layer charge approximations (also applicable to the results of Greene-Kelly and Mg-test) is that the studied samples may not be homogeneous, i.e. they could consist of different layers and thus show intermediate properties. This would explain the inconclusive behaviour in different analyses and can be backed up by evidence of CV values which suggest an irrational order sequence in 9 out of 13 samples. It should be noted however that CV values should be calculated on at least 10 basal peaks (BAILEY, 1982) which were not all present in this case. Furthermore, CV calculations are strongly influenced by inaccurate reading (done by software profile fitting), of the 001 peak position, which is especially true for wider peaks in the case

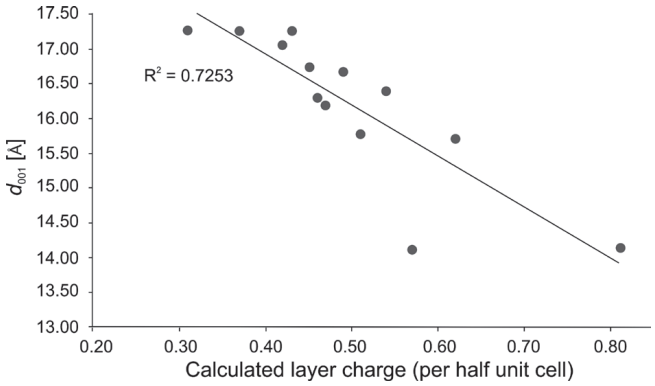

Figure 11. The relationship between calculated and inferred layer charge (after EG-swelling behaviour of K-exchanged samples i.e. observed d_{001}) showing positive correlation with some outliers (notably ŠI1).

of inhomogeneous samples with a small number of smectite layers in stacks.

There are a few samples (most notably ŠI1) where there is a discrepancy between the calculated and observed layer charge (Fig. 11), so for the purposes of classification the observed (inferred) layer charges were used, on account of the fact that the chemical data could be compromised with mineral and amorphous impurities.

When comparing the calculated tetrahedral and octahedral charge with the observed swelling behaviour, the samples largely follow the trend postulated by SATO et al. (1992) (Fig. 12). On their diagram, sample ŠI1, with a higher charge in the tetrahedral sheet, which notably deviated from the linear correlation of calculated and inferred layer charge (Fig. 11) shows behaviour in accordance with the theory that swelling depends not only on the total layer charge but also on its location.

CEC was measured on WR rather than clay-size fractions since all the investigated bentonites are pure enough to not have

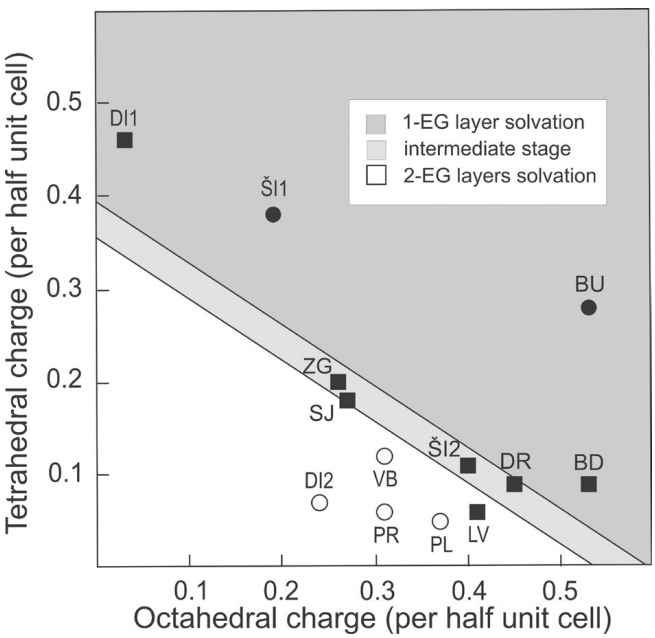

Figure 12. Octahedral and tetrahedral sheet charge and observed swelling behaviour of K-saturated <2 µm sample fractions after EG solvation plotted on the diagram by SATO et al. (1992). White circles – samples fully expanding to about 17 Å; black dots – negligibly expanding samples with 001 peak remaining around 14 Å; black squares –samples showing in-between values.

to be treated before prospective applications. Several samples show CEC values (Table 5) lower than those expected for smectites. MEIER & NÜESCH (1999) denoted the lower CEC limit to be 65 ± 2 cmol(+)/kg; however some samples are even lower than this limit. In this case the issue is most likely due to the fact that WR samples contain variable amounts of mineral and amorphous phases which do not contribute to the CEC.

5.2.2. Structure of the octahedral sheet

When it comes to the octahedral sheet structure, chemical data indicate aluminium abundance. XRD analysis, done on randomly oriented clay-size fraction in the 59 – 65 °2Θ region, showed all the investigated clay minerals to be dioctahedral (Table 3).

Additional cations occupying the octahedral sheet are ferric, ferrous and magnesium cations; the last two contributing to the octahedral charge.

The OH vibrations visible in the FTIR spectra are affected by the octahedral cations to which the OH group is coordinated (PETIT, 2006). The octahedral cation occupancy can be deduced from characteristic bands: around 920 cm^{-1} for AlAlOH, 885 cm^{-1} for AlFeOH and 845 cm^{-1} for AlMgOH. There is a correlation between the octahedral charge and the prominence of the different bands. Beidellites (DI1, DI2 and ŠI1) have a more prominent AlAlOH band and other less prominent bands, while samples with a higher number of octahedral substitutions show other more prominent bands. Samples with a higher amount of octahedral Fe (e.g. BD) can also be distinguished from the FTIR spectra.

Thermal analyses performed on clay-size samples provided additional information about the structure of the octahedral sheet. The nature of octahedral cations and their bonding strength affect the endothermic peak position. The dehydroxylation temperature increases as Fe–OH < Al–OH < Mg–OH (KÖSTER, 1993). DRITS et al. (1995) showed that the temperature depends not only on the mineral species, but also on the position of vacant octahedra in dioctahedral clay minerals. They set the limit of the dehydroxylation peak temperature discriminating between a *trans*-vacant and *cis*-vacant octahedral sheet at 600 °C. This means that ideal *trans*-vacant (*tv*) montmorillonites should lose their OH-groups below 600 and ideal *cis*-vacant (*cv*) montmorillonites above 600 °C. WOLTERS & EMMERICH (2007) expanded on this and postulated a model for estimating the *tv* and *cv* sheets in a given sample. KOMADEL & MADEJOVÁ (2010) stated that beidellitic samples would show a lower dehydroxylation temperature, i.e. more *trans*-vacant sites.

Dehydroxylation temperatures varied significantly between the analysed samples with some samples showing multiple dehydroxylation peaks (Table 6). Generally speaking "ideal" montmorillonites lose their structural water in the 700 °C region, while "ideal" beidellites have their main dehydroxylation peak below 550 °C (GREENE-KELLY, 1953). The fact that some samples cannot be attributed to either group shows that some of the samples are "non-ideal", i.e. structurally inhomogeneous. A small number of samples and their low Fe content did not allow determination of the influence of Fe on the dehydroxylation temperature.

In the present study, the peak modelling of the mass-spectrometer curves of evolved water proposed by WOLTERS & EMMERICH (2007) was not used; however, by observing the peak dehydroxylation temperature it was possible to deduce the predominant nature of the octahedral sheets (Table 6).

The samples in which the dehydroxylation peak was below 550 °C show an exothermic peak around 900 °C attributed to the recrystallization process.

5.2.3. Iron content

BD is the only sample in which Fe made up a considerable proportion of the octahedral cations (almost 20%) and is considered ferrian. Samples coming close to the limit of 15% percent of the octahedral positions occupied by Fe ions are DI1 and ŠI1; however, those would not be considered ferrian, noting as well that other samples taken from the same deposits (DI2 and ŠI2) do not follow the same trend.

Information about Fe speciation, its oxidation state and coordination, is necessary for the correct structural formula calculations. In this study, Mössbauer spectroscopy was used to provide the required data (Table 10). It showed that Fe^{2+} is present in the majority of samples (9 out of 13). Its content is small but in some samples not negligible (> 10 % of total Fe). There is no evident relationship between the geological environment (lacustrine or marine) and the total iron or Fe^{2+} content. Traditionally, in formula calculations, only Al for Si substitutions have been accounted for, mostly due to the smaller ion size of Al in comparison with Fe^{3+}, but also due to the difficulties with $^{IV}Fe^{3+}$ measurement, which persist even in Mössbauer spectroscopy analyses. GATES et al. (2002) concluded that tetrahedral Fe^{3+} is unlikely to be present in smectites with < 34 wt% Fe_2O_3 but KAUFHOLD et al. (2017) found tetrahedral Fe^{3+} even in samples containing 2.1 wt% Fe_2O_3. In sample BD with 6.6 wt% (the highest Fe content among analysed samples) fitting of Mössbauer spectra revealed that 7.4 % of the total iron is present in the tetrahedral coordination. Nevertheless, it must be said that for this sample a reasonable fit could also be obtained without the doublet corresponding to $^{IV}Fe^{3+}$.

Some of the spectra showed only one or one dominant doublet (with a quadrupole splitting value in the range 0.43-0.68 mm/s) characteristic for Fe^{3+} in the octahedral coordination. For others, an additional doublet attributed to Fe^{3+} in the octahedral coordination (with a quadrupole splitting value ranging between 0.87 and 1.24 mm/s) had to be used. Some authors attribute (e.g. COEY, 1980) these two doublets to Fe^{3+} in octahedral *cis*- and *trans*- positions, respectively. Several authors (BARON et al., 2017; PELAYO et al., 2018 and references therein) doubt this interpretation. The studied samples speak in favour of the latter: both BU and ŠI1 samples have only the first doublet and according to the thermal properties the first is *cis*-vacant while the second is *trans*-vacant. Other authors (PELAYO et al., 2018 and references therein) relate these doublets to less and more distorted octahedral environments. PELAYO et al. (2018) attribute distortion to the substitution of Al with Fe but for the studied samples no correlation of total iron content and % area of the second doublet was observed.

Sometimes, a reliable structural formula calculation, including proper iron content evaluation, is problematic due to impurities, especially amorphous ones. In such cases, relationships between chemical and physical properties are used to evaluate the content of an element of interest. An example of such physical properties, which can be easily measured, are unit-cell dimensions. It is known that the length of the *b*-unit cell edge is correlated with structural Fe content (RADOSLOVICH, 1962; BRIGATTI, 1983; KÖSTER et al., 1999; HEUSER et al., 2013).

For the analysed set of samples, most of which have a low iron content, no correlation of Fe content and *b*-unit cell dimension was observed (Fig. 13). There are several possible explanations for this. Such a lack of correlation can be caused by inaccurate structural formulae resulting from impurities present in the sample, e.g. the very low unit cell dimension for given Fe

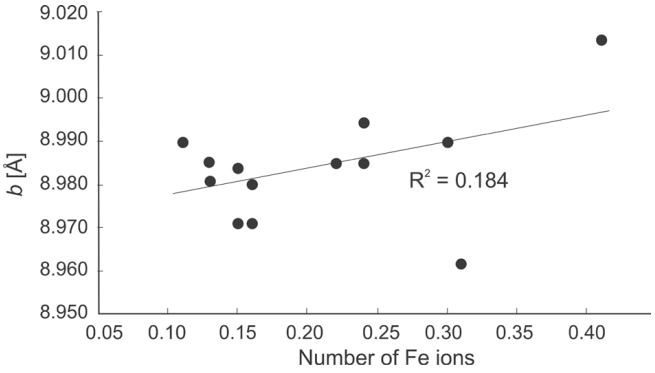

Figure 13. Correlation of *b*-unit cell dimension and number of Fe ions obtained by structural formula calculation.

content for DI2 sample could be because of the presence of amorphous material. Another source of error could be the calculation of the *b*-unit cell dimension by multiplying d_{060}, since the observed reflection is not a single one (DESPRAIRIES, 1983). The lack of correlation could also be explained by the fact that the b-dimension does not depend only on iron content (RADOSLOVICH, 1962), and that for low iron content other factors (octahedral Mg and tetrahedral Al content) can be more important. This is in agreement with the results by BRIGATTI (1983) who stated that correlation of the *b*-unit cell edge with the structural Fe content is valid only for samples with an iron content > 0.50 atoms per half-cell and none of the analysed samples fulfil that requirement. HEUSER et al. (2013) also observed poorer correlation for samples with low Fe contents. In contrast, KÖSTER et al. (1999) do not mention the lack of correlation; however, their regression was determined on only five samples of nontronites and Fe-rich smectites.

Observed *b*-unit cell dimensions were compared with those calculated using different regressions (Table 11, Fig. 14). There is a poor correlation between the observed and calculated values for the regression of KÖSTER et al. (1999), which takes only the influence of Fe into account. Better correlation was observed for values calculated using the regression of RADOSLOVICH (1962), which takes into account other substitutions; however, all calculated values are greater than those observed.

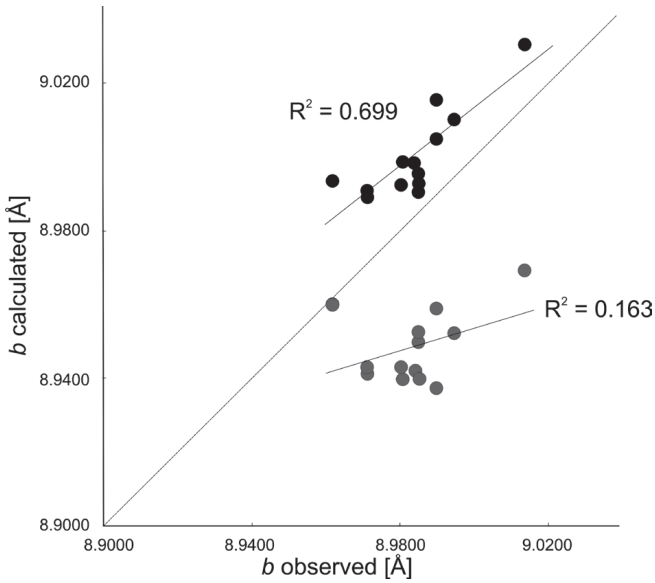

Figure 14. Correlation of observed and calculated *b*-unit cell dimension (black dots – regression of RADOSLOVICH, 1962; gray dots – regression of KÖSTER et al., 1999).

5.2.4. Charge location

Overall (with the exceptions of the SJ, VB and DI2 samples), the Greene-Kelly test results are in accordance with the distribution of layer charge which can be observed from the calculated chemical formulae. They are also predominantly in accordance with the observed dehydroxylation temperatures which are, as expected, lower for beidellitic samples (KOMADEL & MADEJOVÁ, 2010).

Based on the distribution of the layer charge between octahedral and tetrahedral sheets, smectites can be divided into montmorillonites (90–100% of charge originating in octahedral sheet – O), beidellitic montmorillonites (50–89% O), montmorillonitic beidellites (10–49% O) and beidellites (0–9% O) (EMMERICH et al., 2009).

Most of the studied samples fall into the "beidellitic montmorillonite" category, even though their octahedral charge ranges from 57, which is close to "montmorillonitic beidellite" to 88% O which is very close to "montmorillonite". Only DI1 and ŠI1 can be classified as beidellite and montmorillonitic beidellite, respectively. Those two samples are also the only ones consistently showing the higher amount of tetrahedral charge, i.e. other analyses (chemistry, DTA) are in accordance with their beidellitic nature.

5.2.5. Interlayer cations

Chemical analysis and subsequent formula calculation (Table 9) show that Ca is the dominant interlayer cation in the majority of the investigated bentonites. Na is dominant only in two samples (BD and DR), while one sample (VB) shows an approximately equal ratio of Ca and Na in the interlayer. The sample ZG shows quite large quantities of Mg in the interlayer, though this could be a miscalculation due to amorphous impurities (volcanic glass) present in the sample.

DTA results largely confirm the chemical data when it comes to the interlayer cations. The majority of samples (except BD and DR) show a two-step dehydration process. This is in accordance with the fact that in both the BD and DR samples Na is the dominant interlayer cation. According to GREENE-KELLY (1953) and SCHULTZ (1969), Na-smectites show a single endotherm peak around 100-150 °C, while Ca-smectites have two distinct endotherm peaks. According to GREENE-KELLY (1953) this is the result of the premature loss of water during dehydration caused by limited stability of the monolayer Na-smectite complex. In the VB sample in which chemical analysis determined Na and Ca in the interlayer, two distinct peaks are visible, though the higher temperature one is very small.

Samples with Na cations in the interlayer showed an additional endothermic peak at around 850 °C.

The presence of an NH_4Br deformation band in IR spectra of some samples indicates NH_4^+ ions in their interlayer (MADEJOVÁ & KOMADEL, 2001).

6. CONCLUSIONS

Thirteen bentonite samples from eleven known deposits in Croatia, Bosnia and Herzegovina, Serbia and Slovenia contain dioctahedral smectite as the main component. Some of them are almost monomineralic while others contain a number of additional phases (kaolinite, illite, quartz, opal-CT, plagioclase feldspars, calcite, zeolite from the heulandite-clinoptilolite series, amorphous impurities, and organic matter), some of those also being present in the <2 μm fraction.

Table 11. Observed (6 x d_{060}) and calculated (after relationships of RADOSLOVICH, 1962 and KÖSTER et al., 1999) b - unit cell dimensions.

Sample	*b* - observed	*b* – calculated after RADOSLOVICH (1962)	*b* – calculated after KÖSTER et al. (1999)
BU	8.9898	9.0158	8.9377
ZG (S)	8.9712	8.9908	8.9433
BD	9.0138	9.0299	8.9693
DR	8.9946	9.0107	8.9523
ŠI1	8.9898	9.0051	8.9591
ŠI2	8.9808	8.9990	8.9400
SJ	8.9712	8.9900	8.9422
PR	8.9850	8.9952	8.9501
DI1	8.9616	8.9937	8.9602
DI2	8.9850	8.9908	8.9523
LV	8.9838	8.9981	8.9422
VB	8.9802	8.9926	8.9433
PL	8.9850	8.9929	8.9400

s – broad peak with shoulder

Smectites show prominent variations in their crystallochemical properties resulting in different bentonite properties. They were classified (Table 12) according to the newest classification scheme proposed by EMMERICH et al. (2009) based on:

– layer charge – both swelling properties of K-saturated samples and calculated structural formulae showed (in spite of some discrepancies) that samples ranged from those with low layer charge to those with high-layer charge but most are medium to low-charged. Results showed that samples are most probably not homogeneous, i.e. they consist of layers of different charges.

– octahedral sheet structure – all investigated smectites are dioctahedral. IR spectra and chemical analyses showed variations in the Al, Fe and Mg content of the octahedral sheet. Dehydroxylation temperature, as a proxy for the location of the vacancy in the octahedral sheet (*tv* vs. *cv*) varied significantly between the samples with some samples showing multiple dehydroxylation peaks indicating that some of the samples are structurally inhomogeneous.

– iron content – most of the samples are non-ferrian. The exceptions are BD in which Fe accounts for almost 20% of the octahedral cations, and DI1 and ŠI1 samples which are close to the limit defined as 15% percent of the octahedral positions occupied by Fe ions. In the Mössbauer spectrum of the BD sample there is an indication of Fe^{3+} in tetrahedral coordination. Mössbauer spectroscopy showed that Fe^{2+} is present in the majority of samples (9 out of 13). Its content is small but in some samples not negligible (> 10 % of total Fe). Overall, Mössbauer spectra differ significantly between samples.

Table 12. Proposed descriptive names of the smectite mineral dominant in the investigated samples, following classification criteria proposed by EMMERICH et al. (2009).

Sample	Proposed descriptive name				
BU	Ca-saturated	high-charge		*cv*	beidellitic montmorillonite
ZG	Mg,Ca-saturated	medium-charge		*tv/cv*	beidellitic montmorillonite
BD	Na-saturated	medium-charge	ferrian	*tv/cv*	beidellitic montmorillonite
DR	Na- saturated	medium-charge		*cv/tv*	beidellitic montmorillonite
ŠI1	Ca,Mg- saturated	high-charge		*tv*	montmorillonitic beidellite
ŠI2	Ca- saturated	medium-charge		*cv*	beidellitic montmorillonite
SJ	Ca- saturated	medium-charge		*cv/tv*	beidellitic montmorillonite
PR	Ca- saturated	low-charge		*cv*	beidellitic montmorillonite
DI1	Ca- saturated	medium-charge		*tv/cv*	beidellite
DI2	Ca- saturated	low-charge		*cv*	beidellitic montmorillonite
LV	Ca- saturated	medium-charge		*cv*	beidellitic montmorillonite
VB	Ca,Na- saturated	low-charge		*cv*	beidellitic montmorillonite
PL	Ca- saturated	low-charge		*cv*	beidellitic montmorillonite

– charge location – calculated structural formulae, which are in accordance with the results of Greene-Kelly tests and FTIR spectroscopy, showed that most of the samples fall into the "beidellitic montmorillonite" category, even though their octahedral charge ranges from 57%, which is close to "montmorillonitic beidellite" to 88% O (PL sample) which is very close to "montmorillonite". Samples DI1 and ŠI1 contain "beidellite" and "montmorillonitic beidellite, respectively.

– type of interlayer cation - the dominant cation in the interlayer is Ca for most samples, except BD and DR where Na is more abundant and VB in which both cations are present in approximately equal amounts.

ACKNOWLEDGMENT

The research has been financially supported by the 119-1191155-1156 project of the Croatian Ministry of Science and Education and annual support over several years from the University of Zagreb. The authors are grateful to Dobroslav SUPAN†, Stanislav MEĐIMOREC, Franjo PERCELA, Frane MARKOVIĆ and Vanja BIŠEVAC for their help in providing samples and to Dražan JOZIĆ (University of Split, Faculty of Chemistry and Technology) and Dominik CINČIĆ (University of Zagreb, Faculty of Science, Department of Chemistry) for recording thermal curves. The authors also express their gratitude to Anita GRIZELJ and an anonymous reviewer for their valuable constructive comments and suggestions.

REFERENCES

AVANIĆ, R. (2012): Litostratigrafske jedinice donjeg miocena sjeverozapadne Hrvatske [*Lower Miocene lithostratigraphic units from north-western Croatia* - in Croatian with English Summary].– Unpl. PhD Thesis, Faculty of Science, University of Zagreb, 162 p.

BAILEY, S.W. (1982): Nomenclature for regular interstratifications.– Am. Mineral., 67, 394–398. DOI: 10.1180/CLAYMIN.1982.017.2.09

BARON, F., PETIT, S., PENTRÁK, M., DECARREAU, A. & STUCKI, J.W. (2017): Revisiting the nontronite Mössbauer spectra.– Am. Mineral., 102, 1501–1515.

BIŠEVAC, V., ŠEGVIĆ, B., TIBLJAŠ, D. & LUGOVIĆ, B. (2007): Mineralogy of altered tephra layers in the Upper Jurassic Lemeš deposits near Maovice (Dalmatia, Croatia).– In: ROCHA, F., TERROSO, D. & QUINTELA, A. (eds.): Euroclay 2007, Abstract Book. University of Aveiro, Aveiro, 75–76.

BRAUN, K. (1991): Mineraloško-petrografske karakteristike i geneza ležišta bentonitnih glina Maovica, Gornje Jelenske, Bednje i Poljanske Luke [*Mineralogical-petrographical characteristics and genesis of the bentonite deposits of Maovice, Gornja Jelenska, Bednja and Poljanska Luka* – in Croatian, with an English Abstract].– Prirodoslovna istraživanja, 63, Acta Geol., 21/1, 1–34.

BRIGATTI, M.F. (1983): Relationship between composition and structure in Fe-rich smectites.– Clay Miner., 18, 177–186. doi: 10.1180/claymin.1983.018.2.06

BRIGATTI, M.F. & POPPI, L. (1981): A mathematical model to distinguish the members of the dioctahedral smectite series.– Clay Miner., 16, 81–89. doi: 10.1180/claymin.1981.016.1.06

BRINDLEY, G.W. & BROWN, G. (1980): The X-ray identification and crystal structures of clay minerals.– Mineralogical Society, London, 495 p. doi: 10.1180/mono-5

BROWN, G. (1961): The X-ray identification and crystal structures of clay minerals.– Mineralogical Society, Clay Minerals Group, London, 544 p.

CHRISTIDIS, G.E. & EBERL, D.D. (2003): Determination of layer charge characteristics of smectites.– Clay. Clay Miner., 51, 644–655. doi: 10.1346/CCMN.2003.0510607

ČÍČEL, B. & MACHAJDÍK, D. (1981): Potassium- and ammonium-treated montmorillonites. I. Interstratified structures with ethylene glycol and water.– Clay. Clay Miner., 29, 40–46. doi: 10.1346/CCMN.1981.0290106

COEY, J.M.D. (1980): Clay minerals and their transformations studied with nuclear techniques: The contribution of Mössbauer spectroscopy.– Atom. Energy Rev., 18, 73–124.

DESPRAIRIES, A. (1983): Relation entre le parametre *b* des smectites et leur contenu en fer et magnesium. Application a l'etude des sediments.– Clay Miner., 18, 165–175. doi: 10.1180/claymin.1983.018.2.05

DRITS, V.A., BESSON, G. & MULLER, F. (1995): An improved model for structural transformations of heat-treated aluminous dioctahedral 2:1 layer silicates.– Clay. Clay Miner., 43, 718–731. doi: 10.1346/CCMN.1995.0430608

DRŽAJ, B. & LUKACS, E. (1968): Nekatere geološke in tehnološke značilnosti bentonitov iz nahajališč v okolici Celja [*Some geological and technological characteristics of bentonites in deposits from Celje surroundings* – in Slovenian].– Geologija, 11, 129–136.

EMMERICH, K., WOLTERS, F., KAHR, G. & LAGALY, G. (2009): Clay profiling: The classification of montmorillonites.– Clay. Clay Miner., 57, 1, 104–114. doi: 10.1346/CCMN.2009.0570110

GATES, W.P., SLADE, P.G., MANCEAU, A. & LANSON, B. (2002): Site occupancies by iron in nontronites.– Clay. Clay Miner., 50, 223–239. doi: 10.1346/000986002760832829

GREENE-KELLY, R. (1953): Irreversible dehydration in montmorillonite. Part II.– Clay Mineral Bull, 2, 52–56.

GREENE-KELLY, R. (1955): Dehydration of the montmorillonite minerals.– Mineral. Mag., 30, 604–615. doi: 10.1180/minmag.1955.030.228.06

GRIM, R.E. & KULBICKI, G. (1961): Montmorillonite: High temperature reactions and classification.– Am. Mineral., 46, 1329–1369.

GUGGENHEIM, S., ADAMS, J.M., BAIN, D.C., BERGAYA, F., BRIGATTI, M.F., DRITS., V.A., FORMOSO, M.L.L., GALÁN, E., KOGURE, T. & STANJEK, H. (2006): Summary of recommendations of nomenclature committees relevant to clay mineralogy: report of the Association Internationale pour l'Etude des Argiles (AIPEA) Nomenclature Committee for 2006.– Clay Miner., 41, 863–877. doi: 10.1180/0009855064140225

HEUSER, M., ANDRIEUX, P., PETIT, S. & STANJEK, H. (2013): Iron-bearing smectites: a revised relationship between structural Fe, b cell edge lengths and refractive indices.– Clay Miner., 48, 97–103. doi: 10.1180/claymin.2013.048.4.06

KAUFHOLD, S., STUCKI, J.W., FINCK, N., STEININGER, R., ZIMINA, A., DOHRMANN, R., UFER, K., PENTRÁK, M. & PENTRÁKOVÁ, L. (2017): Tetrahedral charge and Fe content in dioctahedral smectites.– Clay Miner., 52, 51–65. doi: 10.1180/claymin.2017.052.1.03

KOMADEL, P. & MADEJOVÁ, J. (2010): Identification and characterization of interstratified clay minerals with spectroscopic and classical methods.– In: FIORE, S, CUADROS, J. & HUERTAS, F.J. (eds.): Interstratified Clay Minerals: Origin, Characterization and Geochemical Significance. AIPEA Educational Series, Pub. No. 1., 89–113.

KÖSTER, H.M. (1993): Beschreibung Einzelner Tonminerale.– In: JASMUND, K. & LAGALY, G. (eds.): Tonminerale und Tone: Struktur, Eigenschaften, Anwendungen und Einsatz in Industrie und Umwelt. Steinkopff Verlag, Darmstadt, 33–58. doi: 10.1007/978-3-642-72488-6_2 doi: 10.1180/claymin.1999.034.4.06

KÖSTER, H.M., EHRLICHER, U., GILG, H.A., JORDAN, R., MURAD, E. & ONNICH, K. (1999): Mineralogical and chemical characteristics of five nontronites and Fe-rich smectites.– Clay Miner., 34, 579–599.

KRIZMANIĆ, K. (1995): Palynology of the Miocene Bentonite from Gornja Jelenska (Mt. Moslavačka Gora, Croatia).– Geol. Croat., 48, 147–154.

KRSTIĆ, N., DUMURDŽANOV, N., OLUJIĆ, J., VUJNOVIĆ, L. & JANKOVIĆ-GOLUBOVIĆ, J. (2001): Interbedded tuff and bentonite in the Neogene lacustrine sediments of the central part of the Balkan Peninsula. A review.– Acta Vulcanologica, 13, 91–99.

KRUMM, S. (1994): Centrifuge, Erlangen.– http://www.ccp14.ac.uk/ccp/web-mirrors/krumm/html/software/winsoft.html

LAGAREC, K. & RANCOURT, D.G. (1998): RECOIL Mössbauer Spectral Analysis Software for Windows.– Department of Physics, University of Ottawa.

MADEJOVÁ, J. & KOMADEL, P. (2001): Baseline studies of the clay minerals society source clays: Infrared methods.– Clay. Clay Miner., 49, 5, 410–432. doi: 10.1346/CCMN.2001.0490508

MANDIC, O., de LEEUW, A., BULIC, J., KUIPER, K.F., KRIJGSMAN, W. & JURIŠIĆ-POLŠAK, Z. (2012): Paleogeographic evolution of the Southern Pannonian Basin: $^{40}Ar/^{39}Ar$ age constraints on the Miocene continental series of Northern Croatia.– Int. J. Earth Sci. (Geol Rundsch), 101, 1033– 1046. doi: 10.1007/s00531-011-0695-6

MARKOVIĆ, S. (2002): Hrvatske mineralne sirovine [*Croatian raw materials* – in Croatian].– Institut za geološka istraživanja, Zagreb, 544 p.

MARKOVIĆ, F., KOVAČIĆ, M., ĆORIĆ, S., TIBLJAŠ, D., PEZELJ, Đ., HAJEK-TADESSE, V., HERNITZ-KUČENJAK, M. & BAKRAČ, K. (2018): Miocene tuffs from the North Croatian Basin.– In: GANIĆ, M., CVETKO, V., VULIĆ, P., ĐURIĆ, D. & ĐURIĆ, U. (eds.): Book of Abstracts 17th Serbian Geological Congress, Vrnjačka Banja, 166–168.

MEIER, L.P., & NÜESCH, R. (1999): The Lower Cation Exchange Capacity Limit of Montmorillonite.– J. Coll. Interf. Sci., 217, 77–85. doi: 10.1006/jcis.1999.6254

MILADINOVIĆ, D. (1976): Bentoniti [*Bentonites* – in Bosnian].– In: VARIĆAK, D. (ed.): Mineralne sirovine Bosne i Hercegovine, Knjiga II, Ležišta nemetala [*Mineral raw materials of Bosnia and Hercegovina, Book II, Deposits of non-metallic raw materials*]. Geoinžinjering Sarajevo, 402–406.

MINATO, H. (1997): Standardization of methods for zeolite speciality determination and techniques for zeolite resources utilization.– In: KIROV, G., FILIZOVA, L. & PETROV, O. (eds.): Natural Zeolites - Sofia '95, PENSOFT, Sofia, 282–292.

MOORE, D.M. & REYNOLDS Jr. R.C. (1997): X-Ray Diffraction and the Identification and Analysis of Clay Minerals.– Oxford University Press, Oxford, 378 p.

PAMIĆ, J. (1997): Vulkanske stijene Savsko-Dravskog međuriječja i Baranje (Hrvatska) [*Volcanic rocks from the Sava-Drava interfluve and Baranja in the South Pannonian Basin (Croatia)* – in Croatian with an English Summary].– Nafta, Zagreb, 192 p.

PANanalytical (2004): X'Pert HighScore Plus, Version 2.1.- Almelo.

PELAYO, M., MARCO, J.F., FERNÁNDEZ, A.M., VERGARA, L., MELÓN, A.M. & PÉREZ DEL VILLAR, L. (2018): Infrared and Mössbauer spectroscopy of Fe-rich smectites from Morrón de Mateo bentonite deposit (Spain).– Clay Miner., 53, 17–28. doi: 10.1180/clm.2018.1

PETIT, S. (2006): Fourier Transform Infrared Spectroscopy.– In: BERGAYA, F., THENG, B.K.G. & LAGALY, G. (eds.): Dev. Clay Sci., Vol. 1. Handbook of Clay Science, Elsevier, Amsterdam, 909–918. doi: 10.1016/B978-0-08-098259-5.00009-3

RADOSLOVICH, E. (1962): The cell dimensions and symmetry of layer-lattice silicates. II. Regression relations.– Am. Mineral., 47, 617–636.

RIHTERŠIČ, J. (1958): Bentoniti v celjski kotlini [*Bentonites in Celje Basin* – in Slovenian].– Geologija, 4–13, 193–196.

RÖGL, F. (1998): Paleogeographic considerations for Mediterranean and Paratethys seaways (Oligocene to Miocene).– Ann. Naturhist. Mus. Wien, 99A, 279–310.

RUSSELL, J.D. & FRASER, A.R. (1994): Infrared methods.– In: WILSON, M.J. (ed.): Clay Mineralogy: Spectroscopic and Chemical Determinative Methods, Chapman & Hall, London, 11–67. doi: 10.1007/978-94-011-0727-3_2

SATO, T., WATANABE, T. & OTSUKA, R. (1992): Effects of layer charge, charge location, and energy change on expansion properties of dioctahedral smectites.– Clay. Clay Miner., 40, 103–113. doi: 10.1346/CCMN.1992.0400111

SCHULTZ, L.G. (1969): Lithium and potassium absorption, dehydroxylation temperature and structural water content of aluminous smectites.– Clay. Clay Miner., 17, 115–149. doi: 10.1346/CCMN.1969.0170302

ŠEGVIĆ, B., TOŠEVSKI, A, ŠTEVANIĆ, D., BIŠEVAC, V. & LUGOVIĆ, B. (2006): Altered tephra layers in the Upper Jurassic Lemeš deposits near Maovice (Dalmatia, Croatia): Clay mineralogy and basic soil mechanic properties.– In: VLAHOVIĆ, I., TIBLJAŠ, D., DURN, G. & BIŠEVAC, V. (eds.): 3rd Mid-European Clay Conference (MECC 06), Abstracts Book. Faculty of Science & Faculty of Mining, Geology and Petroleum Engineering, Zagreb, 104–104.

SIMIĆ V. (2001): Bentoniti i bentonitske gline Srbije – stanje i perspektiva [*Bentonites and bentonitic clays of Serbia – Actual state and prospects* – in Serbian with an English Abstract].– Zbornik radova III međunarodnog savetovanja o površinskoj ekspolataciji glina, Ruma, 186–191.

SIMIĆ, V., ŽIVOTIĆ, D., ANDRIĆ, N., RADOSAVLJEVIĆ-MIHAJLOVIĆ, A. & KAŠIĆ, V. (2014): Zeolite deposits and occurrences in Serbia – an overview.– In: ZEOLITE 2014, 9th International Conference on the Occurrence, Properties and Utilization of Natural Zeolites, Belgrade, Serbia, 217–218.

ŚRODOŃ, J. (1980): Precise identification of illite/smectite interstratifications by X-ray powder diffraction.– Clay. Clay Miner., 28, 401–411.

STARKEY, H.C., BLACKMON, P.D. & HAUFF, P.L. (1984): The Routine Mineralogical Analysis of Clay-Bearing Samples.– U.S. Geol. Surv. Bull., 1563, Washington, 32 p.

STEVENS, R.E. (1946) A system for calculating analyses of micas and related minerals to end members.– Contributions to Geochemistry, 1942-45. Geol. Surv. Bull., 950, 101–119.

TIBLJAŠ, D. (1996): Zeoliti i drugi produkti alteracijskih procesa u oligocenskim i donjomiocenskim piroklastitima na širem području Macelja [*Zeolites and the other products of the alteration processes in Oligocene and Early Miocene pyroclastic rocks from the Macelj area* – in Croatian, with an English Summary].– Unpl. PhD Thesis, Faculty of Science, University of Zagreb, 167 p.

TRUBELJA, F. & BARIĆ, LJ. (1979): Minerali Bosne i Hercegovine [*Minerals of Bosnia and Herzegovina* – in Croatian, with an English Summary].– Zemaljski muzej BiH, Sarajevo, 236–245.

VLAHOVIĆ, I., TIŠLJAR, J., VELIĆ, I. & MATIČEC, D. (2005): Evolution of the Adriatic Carbonate Platform: Palaeogeography,main events and depositional dynamics.– Palaeogeogr. Palaeocl., 220, 333–360. doi: 10.1016/j.palaeo.2005.01.011

VUJNOVIĆ, L. (1981): Osnovna geološka karta SFRJ 1:100000. Tumač za list Bugojno L33−143 [*Basic Geological Map of SFRY 1:100000, Geology of the Bugojno sheet* – in Bosnian, with an English Summary].– Savezni geološki zavod, Beograd, 58 p.

VUKANOVIĆ, M., DIMITRIJEVIĆ, N., DIMITRIJEVIĆ, M.N., KARAJIČIĆ, LJ. & RAKIĆ, M.O. (1977): Osnovna geološka karta SFRJ 1:100000. Tumač za list Vranje L34−54 [*Basic Geological Map of SFRY 1:100000, Geology of the Vranje sheet* – in Serbian, with an English Summary].– Savezni geološki zavod, Beograd, 53 p.

WINCHESTER, J.A. & FLOYD, P.A. (1977): Geochemical discrimination of different magma series and their differentiation products using immobile elements.– Chem. Geol., 20, 325–343. doi: 10.1016/0009-2541(77)90057-2

WOLTERS, F. & EMMERICH, K. (2007): Thermal reactions of smectites – Relation of dehydroxylation temperature to octahedral structure.– Thermochim. Acta, 462, 80–88. doi: 10.1016/j.tca.2007.06.002